is the fact that the calculated fractional change has the correct sign; that is, the calculation yields a higher ordering temperature for He^3 than for He^4.

To summarize, the occurrence of a higher ordering temperature for He^3 can be understood as follows. Because the relative strength of the tunneling term is so small, the transition temperature of the adsorbed system essentially scales with the nearest-neighbor-interaction strength as in a classical system. The major quantum-mechanical effect is to cause this strength to be greater for He^3, as the less localized wave functions of the lighter atoms give greater weight to the repulsive part of the interatomic potential.

ACKNOWLEDGMENTS

The authors wish to thank A. D. Novaco for computing the relevant matrix elements and J. G. Dash and O. E. Vilches for useful discussions.

BFY02850 *PG PLRAA,00JUL3AB320003R020

*Work supported in part by the National Science Foundation.

[1]M. Bretz, J. G. Dash, D. C. Hickernell, E. O. McLean, and O. E. Vilches, Phys. Rev. A (to be published).
[2]See, for example, C. Domb, Philos. Mag. Suppl. **9**, 149 (1960).
[3]C. E. Campbell and M. Schick, Phys. Rev. A **5**, 1919 (1972).
[4]This density range lies between 0.05 and 0.08 $Å^{-2}$.
[5]Y. C. Cheng and M. Schick, Phys. Rev. A **7**, 1771 (1973).
[6]See, for example, W. J. Mullin, Phys. Rev. A **4**, 1247 (1971).
[7]C. N. Yang, Rev. Mod. Phys. **34**, 694 (1962).
[8]P. C. Hohenberg, Phys. Rev. **158**, 383 (1967).
[9]H. A. Bethe, Proc. R. Soc. Lond. **150**, 552 (1935).
[10]R. E. Peierls, Proc. Camb. Philos. Soc. **32**, 471 (1935).
[11]See Ref. 6, wherein perturbation theory is carried out for the ground state to order γ^4.
[12]C. E. Easthope, Proc. Camb. Philos. Soc. **33**, 502 (1937).
[13]P. W. Anderson, Phys. Rev. **80**, 922 (1950).
[14]Y. -Y. Li, Phys. Rev. **84**, 721 (1951).
[15]T. Matsubara and H. Matsuda, Prog. Theor. Phys. **16**, 569 (1956).
[16]D. E. Beck, Mol. Phys. **14**, 311 (1969).
[17]P. E. Phillipson, Phys. Rev. **125**, 1981 (1962).
[18]A. D. Novaco (private communication).
[19]The experimental values of δT and T separately are 0.08 and 2.95 K.

PHYSICAL REVIEW A VOLUME 8, NUMBER 1 JULY 1973

Semiclassical Theory of Saturated Absorption in Gases

Jon H. Shirley
Quantum Electronics Division, National Bureau of Standards, Boulder, Colorado 80302
(Received 5 February 1973)

A three-dimensional theory for the resonant interaction of electromagnetic waves with a gas of two-level atoms is formulated in terms of macroscopic variables. The theory is utilized to find the steady-state attenuation of a plane wave in the presence of another plane wave running in the opposite direction with different amplitude. Contributions are included from the reflection of the oppositely running wave by an induced standing-wave inhomogeneity in the population inversion of the medium. The resulting attenuation and reflection coefficients are expressed as velocity integrals of continued fractions. Correspondence is made with existing gas-laser theories, yielding the formulation of a high-intensity ring-laser theory. Analytic approximations for the coefficients are presented for the Doppler-limit cases of both waves weak, one wave weak, and negligible reflection (rate-equation approximation). More-general cases have been calculated numerically. The attenuation coefficients exhibit a Lamb-dip feature. The relative depth of the dip increases rapidly with power at low saturation levels, slowly at high saturation, and is greater in the attenuation of the weaker wave. The width of the dip is nonlinearly power broadened. The shape of the dip is very nearly Lorentzian, except for one special case at high power in which the line splits. The propagation equations for the two waves are integrated over long absorption paths. A large resulting attenuation increases the relative size of the dip while decreasing the power broadening.

I. INTRODUCTION

Saturated absorption, or the nonlinear absorption of electromagnetic radiation at high power levels, was first observed in gases by microwave spectroscopy.[1] As the incident power was increased, the percent absorption decreased and the width of the absorption line increased. A theoretical explanation of these effects was given by Karplus and Schwinger[2] and independently by Snyder and Richards.[3] Actually such effects first appeared in the so-called Rabi transition probability[4] long used by workers in atomic and molecular beam resonance spectroscopy. Similar

saturation effects are also well known in magnetic resonance[5] and other forms of radio-frequency spectroscopy.[6,7]

The recent development of lasers has permitted the observation of saturation at infrared and optical frequencies. The predominance of inhomogeneous broadening (Doppler broadening for gases) at these higher frequencies leads to a new phenomenon associated with the concept of "hole burning."[8] When a gaseous system is subject to a resonant standing-wave field, a narrow spectral feature may occur having only the homogeneous linewidth. This feature was predicted mathematically by Rautian[9] and in Lamb's fundamental paper on the theory of the gas laser.[10] When observed in the output power of a gas laser, this feature is commonly referred to as the "Lamb dip." A saturable absorbing medium within a laser cavity may produce the same feature with opposite sign or an "inverted Lamb dip."[11,12] Similar features have been observed in the fluorescence from a saturated level,[13] or in the amplification of a laser beam by a second laser oscillating on a different transition with a common level.[14] By directing laser beams in opposite directions through an external absorption cell,[15,16] Lamb-dip features can be seen without worrying about threshold conditions or the nonlinear behavior of an active laser medium. Altogether these techniques have shown exciting potential for studies in spectroscopy,[17-21] collision broadening,[22,23] and frequency stabilization.[24-26] A theoretical understanding of saturated absorption is desirable for the interpretation of these experiments.

The present paper provides a theoretical model for the interaction of a gaseous two-level medium with two oppositely running waves of arbitrary amplitude. Mathematically it is an extension of the theory of high-intensity gas lasers[27-29] to the case of running waves of unequal amplitude, but treated from the point of view of absorption. Some known results are included for completeness and perspective. The emphasis in the new work is on the amplitude and width of the Lamb-dip feature as affected by the intensities of the two waves and the optical depth of the absorption cell. The results are valid for steady-state conditions with unbounded plane-wave fields of the same frequency and polarization. The model is also restricted to those relaxation processes describable by simple velocity-independent decay constants. The interesting case of a three-level medium excited by two resonant frequencies has been treated elsewhere.[7,30-32]

In Sec. II we present a general three-dimensional formulation of the interaction of electromagnetic waves with a gas of two-level atoms. By using macroscopic variables no explicit mention of the density matrix is required. However, the theory is based on the same physical assumptions and is mathematically equivalent to the density-matrix theories. It is presented here for its generality and relative simplicity.

In Sec. III we review the saturated absorption of a single running wave. The heart of the paper is Sec. IV, where we find general expressions for the attenuation and reflection coefficients for two oppositely running waves. Several special cases are treated analytically, while the more general case is studied numerically. The results are related to existing theories of high-intensity standing-wave gas lasers[27-29] and yield as a bonus a formulation for a high-intensity ring laser. In Sec. V we numerically integrate the propagation equations over the length of an absorption cell to find the resulting enhancement of the Lamb-dip feature. Section VI summarizes some of the experimental implications of the results.

II. MACROSCOPIC VARIABLE FORMULATION

The following theory is essentially a generalization of the author's elementary maser theory.[33] To the time-dependent macroscopic variables used previously we add spatial and velocity dependence. The resulting equations of motion encompass a much wider range of phenomena, but are correspondingly much more difficult to solve.

In our earlier paper we started with the electromagnetic field quantized and went over to a semiclassical theory by neglecting correlations between the atoms and field. This approach permitted a determination of the validity of the semiclassical approximation by evaluating the correlations.[34] On the strength of those results we shall in this paper consider the electromagnetic field to be classical from the start. Since our medium will have a nonlinear susceptibility, we explicitly separate the medium polarization from the electric displacement. Maxwell's equations for a charge-free nonmagnetic material then give the following equation of motion for the electric field:

$$\frac{\partial^2 \vec{E}}{\partial t^2} + 2\gamma_c \frac{\partial \vec{E}}{\partial t} - c^2 \nabla^2 \vec{E} = -\frac{1}{\epsilon_0} \frac{\partial^2 \vec{P}}{\partial t^2}, \tag{1}$$

where $\vec{E}$ and $\vec{P}$ are functions of position $\vec{r}$ and time t. The damping coefficient γ_c may arise from a finite conductivity of the medium or be absent. For magnetic dipole transitions a similar equation holds for the magnetic field driven by the magnetization.

For the nonlinear medium we assume a large

number of identical atoms or molecules located at positions $\vec{r}_j$ and traveling with constant velocities $\vec{v}_j$. For each atom we shall be concerned with only two internal states which will be resonantly coupled to the electromagnetic field. We therefore represent the Hamiltonian for each atom by a two-by-two matrix:

$$\mathcal{H}_j = \tfrac{1}{2}\hbar\omega_0 \sigma_j^z - \vec{\mu}\cdot\vec{E}_j(\vec{r}_j, t)\sigma_j^x \ . \tag{2}$$

Here $\hbar\omega_0$ is the energy difference between the two levels, $\vec{\mu}$ is the induced dipole moment, $\vec{E}_j$ is the classical field strength evaluated at the position of the jth atom and the σ's are Pauli spin matrices, independent for each j. The average energy of the two levels is omitted since it does not contribute to the dynamics. Only one polarization of the field $\vec{E}$ will be considered, μ and E henceforth being written as scalars.[35] Treating the Pauli spin matrices as time-dependent operators, we find the Heisenberg equations of motion

$$\begin{aligned} \frac{d}{dt}\sigma_j^x &= -\omega_0\sigma_j^y \ , \\ \frac{d}{dt}\sigma_j^y &= \omega_0\sigma_j^x + \frac{2\mu E_j}{\hbar}\sigma_j^z \ , \\ \frac{d}{dt}\sigma_j^z &= -\frac{2\mu E_j}{\hbar}\sigma_j^y \ . \end{aligned} \tag{3}$$

In the Lagrangian description of fluid mechanics the motion of individual particles is followed. This view has been the starting point of most formulations of gas-laser theory. In the Eulerian description, the properties of particles at a fixed position are studied regardless of which particles happen to be there or how they got there. This latter approach has been fruitful for fluid dynamics and we adopt it here. In this view we can, for example, define the density of atoms of a given velocity as a sum over all atoms with δ-function contributions from each:

$$N(\vec{r}, \vec{v}, t) = \sum_j \delta(\vec{r} - \vec{r}_j)\,\delta(\vec{v} - \vec{v}_j) \ . \tag{4}$$

The function N is then interpreted as a continuous function of $\vec{r}$ and $\vec{v}$ by considering its variation only over distances and velocities large compared to atomic separations and velocity differences. In other words N is just the total number of atoms times the Boltzmann function $f(\vec{r}, \vec{v}, t)$ of kinetic theory.

We introduce our other macroscopic variables in an analogous way by adding to N information about the internal states of the atoms[36]:

$$\begin{aligned} P(\vec{r}, \vec{v}, t) &= \sum_j \mu\langle\sigma_j^x\rangle\,\delta(\vec{r} - \vec{r}_j)\,\delta(\vec{v} - \vec{v}_j) \ , \\ Q(\vec{r}, \vec{v}, t) &= \sum_j \mu\langle\sigma_j^y\rangle\,\delta(\vec{r} - \vec{r}_j)\,\delta(\vec{v} - \vec{v}_j) \ , \\ W(\vec{r}, \vec{v}, t) &= \sum_j \langle\sigma_j^z\rangle\,\delta(\vec{r} - \vec{r}_j)\,\delta(\vec{v} - \vec{v}_j) \ . \end{aligned} \tag{5}$$

The angular brackets represent quantum-mechanical expectation values. W is the population inversion density. P and Q are the in-phase and quadrature components of the macroscopic electric polarization. When integrated over velocity, P becomes the source function for (1). These variables now represent the macroscopic properties of the medium without reference to individual atoms.

The equations of motion for these variables are obtained from their total time derivatives. If we consider the atoms to have classical linear trajectories between collisions, then $\vec{r}_j$ has the form $\vec{r}_{j0} + \vec{v}_j t$. Using the properties of δ functions, the time derivative acting on $\vec{r}_j$ can be rewritten as a space derivative and transferred to the left-hand side to make up the substantive or material derivative. From (4) we thus obtain the Boltzmann equation for force-free noninteracting particles

$$\left(\frac{\partial}{\partial t} + \vec{v}\cdot\nabla\right) N = 0 \ . \tag{6}$$

With the aid of (3), we find for the other variables (5)

$$\begin{aligned} \left(\frac{\partial}{\partial t} + \vec{v}\cdot\nabla\right) P &= -\omega_0 Q \ , \\ \left(\frac{\partial}{\partial t} + \vec{v}\cdot\nabla\right) Q &= \omega_0 P + \frac{2\mu^2 E}{\hbar} W \ , \\ \left(\frac{\partial}{\partial t} + \vec{v}\cdot\nabla\right) W &= \frac{2}{\hbar} QE \ . \end{aligned} \tag{7}$$

The first of these equations could be used to eliminate Q from the other two, producing a second-order equation for P. For stationary atoms ($\vec{v}\cdot\nabla$ terms omitted), Eqs. (7) would then be the same as those used by Oraevskii,[37] Jaynes and Cummings,[38] or Davis.[39] The $\vec{v}\cdot\nabla$ term is a convenient way of including the time-dependent interaction seen by atoms moving through a spatially varying field and avoids the extra time variable sometimes introduced.[27,29] Although its use in laser theory is not new,[40] only recently have authors taken advantage of it.[28,32,41-44]

In the important case that E is a nearly monochromatic wave of angular frequency ω, the basic equations (7) can be simplified by removing their rapid time dependence. Let us introduce complex amplitudes by defining

$$P(\vec{r}, \vec{v}, t) - iQ(\vec{r}, \vec{v}, t) = 2\mu M(\vec{r}, \vec{v}, t)\, e^{-i\omega t} \ , \tag{8}$$

$$E(\vec{r}, t) = E_0 A(\vec{r}, t)\, e^{-i\omega t} + \text{c.c.}, \tag{9}$$

$$b = \mu E_0/\hbar \ . \tag{10}$$

Then the first two equations of (7) can be combined

into

$$\left(\frac{\partial}{\partial t}+\vec{v}\cdot\nabla\right)M=i(\omega-\omega_0)M-ibWA\,, \tag{11}$$

while the third becomes

$$\left(\frac{\partial}{\partial t}+\vec{v}\cdot\nabla\right)W=-2ibMA^*+\text{c.c.} \tag{12}$$

Rapidly varying terms containing $e^{\pm 2i\omega t}$ have been dropped (rotating wave approximation) so that A, M, and W are now assumed to vary with t much more slowly than the carrier frequency ω. The validity of this approximation is very good for $b|A|\ll\omega$.[45] We similarly rewrite (1) in terms of A, retaining only the slowly varying terms (cf. the Appendix of Ref. 33). Using $E_0=(\hbar\omega/2\epsilon_0 V)^{1/2}$, where V is a normalization volume for the field, we obtain

$$\left(\frac{\partial}{\partial t}+\gamma_c+\frac{\omega^2+c^2\nabla^2}{2i\omega}\right)A=ibV\int M(\vec{r},\vec{v},t)\,d^3v. \tag{13}$$

The ∇^2 term allows for the propagation of the wave, including diffraction effects. The parameter b corresponds to the field-atom coupling constant in a treatment quantizing the field.[33] Similarly $|A|^2$ is the mean photon number in the volume V. The real and imaginary parts of M correspond to the variables C and S of Lamb.[10]

In (11) and (12) the atoms are considered free of external influences other than the applied field. A more realistic model includes the dissipative effects of finite-level lifetimes and atomic collisions. For mathematical tractability we shall include dissipation in the simplest way, by adding phenomenological damping and source terms to our equations. To allow for different lifetimes of the upper and lower states, it is necessary to write separate equations for their individual populations. Defining these by

$$N_a=\tfrac{1}{2}(N+W)\ \text{and}\ N_b=\tfrac{1}{2}(N-W)\,,$$

we expand (11) and (12) to

$$\left(\frac{\partial}{\partial t}+\vec{v}\cdot\nabla+\gamma_a\right)N_a=\gamma_a N_a^0-ibMA^*+ibM^*A, \tag{14}$$

$$\left(\frac{\partial}{\partial t}+\vec{v}\cdot\nabla+\gamma_b\right)N_b=\gamma_b N_b^0+ibMA^*-ibM^*A, \tag{15}$$

$$\left(\frac{\partial}{\partial t}+\vec{v}\cdot\nabla+\gamma_2\right)M=i(\omega-\omega_0)M-ib(N_a-N_b)A. \tag{16}$$

Here N_a^0 and N_b^0, which may depend on $\vec{r}$, $\vec{v}$, and t, are the equilibrium values of N_a and N_b occurring in the absence of the field A. Also, γ_a and γ_b are the relaxation rates of the upper and lower states, respectively, while γ_2 is the relaxation rate for the polarization (γ_2 corresponds to $1/T_2$ in magnetic resonance theory[5]). The use of three different relaxation rates accommodates both finite-level lifetimes and hard collisions.[42,46] Soft collisions leading to velocity diffusion[47] or velocity changes correlated with internal state changes[48,49] are not included. The rates are restricted by[42]

$$\gamma_2\geq\tfrac{1}{2}(\gamma_a+\gamma_b)\,, \tag{17}$$

the equality holding in the absence of phase perturbing collisions. Readers familiar with density-matrix formulations will recognize (14)–(16) since

$$\begin{pmatrix} N_a & Me^{-i\omega t} \\ M^*e^{i\omega t} & N_b \end{pmatrix}$$

is just the total number of atoms times the ensemble-averaged density matrix $\rho(\vec{r},\vec{v},t)$ used by Lamb[10] or Feldman and Feld.[28]

Equations (13)–(16) form a complete set of coupled partial differential equations for the interaction of electromagnetic waves with a gas of two-level atoms. They can describe such diverse phenomena as laser oscillators and amplifiers, pulse propagation, self-induced transparency, self-focusing, atomic beam spectrometers, and saturated absorption. They can be used for multimode problems by including the beat notes in A (provided the beat-note frequencies are small compared to ω). They must be generalized for problems involving more than two atomic states or additional frequencies not close to ω (parametric oscillators, harmonic generation).

III. ATTENUATION OF SINGLE RUNNING WAVE

Before attacking our main problem we introduce some of the techniques by applying our general theory to the saturated absorption of a single plane wave propagating in the z direction. We can represent such a wave by the field

$$E=E_1\cos(kz-\omega t-\phi)=E_1\,\mathrm{Re}(e^{ikz}e^{-i\omega t}e^{-i\phi}),$$

where E_1 and ϕ are slowly varying functions both in time and in space (over a wavelength). Comparing with (9) we see that A will have the form of a slowly varying function times e^{ikz}. Just as we removed the rapid time dependence in the preceding section, we now remove this rapid spatial dependence from our equations by defining

$$A=A_1e^{ikz}\ \text{and}\ M=M_1e^{ikz},$$

where A_1 and M_1 are slowly varying both in time and space. Equations (13)–(16) then become

$$\left(\frac{\partial}{\partial t}+\gamma_c+c\frac{\partial}{\partial z}+\frac{c^2\nabla^2}{2i\omega}\right)A_1=ibV\int M_1\,d^3v, \tag{18}$$

$$\left(\frac{\partial}{\partial t}+\vec{v}\cdot\nabla+\gamma_a\right)N_a=\gamma_a N_a^0-ibM_1A_1^*+ibM_1^*A_1, \quad (19)$$

$$\left(\frac{\partial}{\partial t}+\vec{v}\cdot\nabla+\gamma_b\right)N_b=\gamma_b N_b^0+ibM_1A_1^*-ibM_1^*A_1\ , \quad (20)$$

$$\left(\frac{\partial}{\partial t}+\vec{v}\cdot\nabla+ikv_z+\gamma_2\right)M_1=i(\omega-\omega_0)M_1-ib(N_a-N_b)A_1\ . \quad (21)$$

In (18) the z derivative term describes the change in amplitude of the wave while it propagates, while the smaller ∇^2 term primarily describes diffraction by altering the phase front. In (21) the ikv_z term arises from $\vec{v}\cdot\nabla$ acting on e^{ikz}. Considered with the $i\omega_0$ term, it gives the Doppler shift seen by moving atoms.

Equations (18)–(21) describe the propagation through a resonant medium of either continuous waves or pulses of any shape long compared to a wavelength. They are equivalent to Eqs. (44) of Icsevgi and Lamb,[50] who have given a thorough treatment of their solution. Here we reiterate just the solution for a steady-state plane wave. In this case we drop all time derivatives and also the $\vec{v}\cdot\nabla$ and ∇^2 terms which will be small. Equations (19)–(21) are then algebraic equations whose solution is

$$W=N_a-N_b=(N_a^0-N_b^0)[1+2\alpha/(1+T^2)]^{-1}\ , \quad (22)$$

$$M_1=-i(b/\gamma_2)(N_a-N_b)A_1(1-iT)^{-1}, \quad (23)$$

where we have used the abbreviations $T=(\omega-\omega_0-kv_z)/\gamma_2$ for the detuning,

$$\alpha=2b^2|A_1|^2/\gamma_1\gamma_2 \quad (24)$$

for the field intensity parameter, and

$$\gamma_1=2\gamma_a\gamma_b/(\gamma_a+\gamma_b) \quad (25)$$

for the effective relaxation rate of the population inversion W. The α term in (22) represents Bennett's "hole"[8] "burned" in the velocity distribution of population inversion by the saturating wave. In thermal equilibrium, the unsaturated inversion can be written

$$N_a^0-N_b^0=\overline{W}f_M(\vec{v}), \quad (26)$$

where

$$f_M(\vec{v})=\pi^{-3/2}u^{-3}e^{-\vec{v}^2/u^2} \quad (27)$$

is the Maxwell velocity distribution and the mean population inversion density

$$\overline{W}=-(N_a^0+N_b^0)\tanh(\hbar\omega_0/2kT)$$

is negative for an absorbing medium.

The propagation equation (18) then becomes

$$\left(\frac{\partial}{\partial z}+\frac{\gamma_c}{c}\right)A_1=i\left(\frac{bV}{c}\right)\int M_1d^3v\equiv-\beta A_1\ , \quad (28)$$

where the attenuation coefficient β is

$$\beta=\frac{b^2V(-\overline{W})}{c\gamma_2}\int\frac{(1+iT)f_M(\vec{v})\,d^3v}{1+2\alpha+T^2}\ . \quad (29)$$

In the integrand, T depends on v_z only, so the integrations over v_x and v_y can be done trivially. The integral over v_z can be expressed in terms of the real and imaginary parts Z_r and Z_i of the plasma dispersion function[51] yielding

$$\beta=\pi^{-1/2}\beta_0[Q^{-1}Z_i(\zeta)-iZ_r(\zeta)]\ , \quad (30)$$

where

$$\beta_0=\frac{\pi^{1/2}b^2V(-\overline{W})}{cku}=\frac{\pi^{1/2}}{2}\frac{\mu^2(-\overline{W})}{\hbar\epsilon_0 u}\ , \quad (31)$$

$$Q=(1+2\alpha)^{1/2}\ , \quad (32)$$

and the complex argument of the plasma dispersion function is

$$\zeta=(\omega-\omega_0+i\gamma_2Q)/ku\equiv\xi+i\eta Q\ . \quad (33)$$

The real part of β gives the attenuation, while the imaginary part produces a phase shift equivalent to a change in the index of refraction (anomalous dispersion). The real part of the result (30) is included in the paper of Icsevgi and Lamb[50] and was found for the case $\omega=\omega_0$ by Gordon, White, and Rigden.[52]

Note that from (28) A_1 is slowly varying over a wavelength if $|\beta|\ll k$. This condition also justifies neglecting the z components of the $\vec{v}\cdot\nabla$ and ∇^2 terms and will be assumed to hold in the remainder of this paper.

The plasma dispersion function simplifies in two special cases corresponding to the limits of homogeneous and inhomogeneous broadening. The former case, represented by $ku\ll\gamma_2$, is usually valid in microwave spectroscopy. Only a very few extremely fast atoms have appreciable Doppler shifts, that is, the atoms are effectively stationary. We can evaluate this case by replacing $f_M(\vec{v})$ in (29) by a δ function:

$$\beta\simeq\frac{\beta_0}{\pi^{1/2}}\frac{ku}{\gamma_2}\frac{(1+i\tan\psi)}{(Q^2+\tan^2\psi)}\ , \quad (34)$$

where

$$\tan\psi=(\omega-\omega_0)/\gamma_2 \quad (35)$$

is the detuning parameter. The appearance of Q^2 in the denominator instead of 1 broadens the homogeneous line shape and reduces the attenuation at line center. The real part of (34) is essentially the result of Karplus and Schwinger[2] or Snyder and Richards[3] and explains the observations of Townes[1] and the more detailed ones of Carter and Smith.[53]

In the inhomogeneous limit $ku\gg\gamma_2$, most atoms have Doppler shifts so large that they are not in

resonance with the field. The integral in (29) averages over all nearly resonant atoms with $f_M(\vec{v})$, a slowly varying weight function. For $\eta Q \ll 1$ we have the approximation

$$\beta \simeq \beta_0 e^{-\xi^2}(Q^{-1} + 2i\pi^{-1/2}\int_0^{\xi} e^{t^2} dt) . \quad (36)$$

The real part of (36) has just the Doppler line shape reduced by the factor Q at high powers. Note that in the homogeneous case (34), saturation reduces absorption by Q^2 at resonance and not at all off resonance. In the inhomogeneous case (36), the average over detunings gives an intermediate saturation factor.

If we consider small enough detuning so that $\xi \ll 1$, (36) reduces to

$$\beta \simeq \beta_0/Q, \quad (37)$$

independent of tuning. We shall call this approximation the Doppler limit.[10] It can be obtained from (29) by replacing $f_M(\vec{v})$ by $f_M(0)$ and will be used for all our analytic results in Sec. IV. Thus β_0, defined in (31), is the unsaturated attenuation coefficient in the Doppler limit (or at resonance). For the real part of β the Doppler-limit approximation is improved by multiplying by $e^{-\xi^2}$, but the imaginary part of order ξ is not included.

IV. ATTENUATION OF TWO OPPOSITELY RUNNING WAVES

Consider now the medium to be subject to two plane waves of the same frequency, one running in the positive z direction and one in the negative z direction. The field amplitude A then has the form

$$A_1 e^{ikz} + A_{-1} e^{-ikz} , \quad (38)$$

where the amplitudes of the individual waves A_1, A_{-1} are slowly varying functions of z and t. For notational convenience we introduce the relative amplitude λ by

$$A_{-1} = -\lambda A_1 . \quad (39)$$

Generally λ would be complex. However, by shifting the origin of the z coordinate we can arrange to have λ real and positive (A_1 remains complex). Then A can be written as the sum of a standing wave and a residual running wave

$$A = 2i\lambda A_1 \sin kz + (1-\lambda) A_1 e^{ikz} . \quad (40)$$

The zero of z now occurs at a node of the standing wave in correspondence with laser theories.

Some of the problems encountered with two running waves can be illustrated by the case of stationary atoms where an analytic solution is possible. Accordingly we discuss this case in Sec. IV A and then develop the complete formal solution for moving atoms in IV B. Section IV C explains the relationship of our free-running-wave theory to existing laser theory. Much of the character of the solution for moving atoms is revealed by three approximations leading to analytic results presented in Secs. IV D, IV E, and IV F. Some numerical results are given in Secs. IV G and IV H.

A. Stationary Atoms

Let us substitute (38) for A in (14)–(16). For zero-velocity atoms and a steady state the derivative terms vanish and the equations solve algebraically. The result is the same as (22) and (23) except that A_1 is replaced by (38), T is replaced by $\tan\psi$, and α is multiplied by $1-2\lambda\cos^2 kz + \lambda^2$. The last change means that both the polarization M and the inversion density W have a rapid periodic variation in z imposed on them by the standing-wave nature of A. We can represent this variation by Fourier-series expansion:

$$M = \sum_n M_n e^{inkz}, \quad n \text{ odd} , \quad (41)$$

$$W = \sum_n W_n e^{inkz}, \quad n \text{ even} . \quad (42)$$

Since W is real, $W_{-n} = W_n^*$. Of course M and W may also have a slow secular variation in z because of such variations in the driving field A. This can be accommodated by considering the Fourier coefficients to be slowly varying functions of z defined by an integral over one wavelength about any value of z.

Now we insert (38) into the propagation equation (13). Omitting the time derivative, conduction loss, and diffraction terms leaves

$$c\left(\frac{\partial A_1}{\partial z}\right) e^{ikz} - c\left(\frac{\partial A_{-1}}{\partial z}\right) e^{-ikz} = ibV\int M\, d^3v. \quad (43)$$

If A_1 and A_{-1} are to be slowly varying in z, they must be driven only by those components of M with the corresponding rapid spatial variation. By equating Fourier coefficients, we find

$$\frac{\partial A_1}{\partial z} = \frac{ibV}{c}\int M_1 d^3v ,$$
$$-\frac{\partial A_{-1}}{\partial z} = \frac{ibV}{c}\int M_{-1} d^3v . \quad (44)$$

Thus it is only the two Fourier coefficients $M_{\pm 1}$ of the polarization that are effective in driving the field.

It has been common practice in laser theory to describe the saturation effects in terms of the population inversion instead of the polarization. If we equate individual Fourier coefficients in the static solution of (16), we find

$$M_1 = -i(b/\gamma_2)(1 - i\tan\psi)^{-1}(W_0 A_1 + W_2 A_{-1})$$

and a similar expression for M_{-1}. Two terms contribute to M_1. The first is the normal attenuation term proportional to A_1 and the average population inversion W_0. The second term is proportional to the amplitude A_{-1} of the wave running in the opposite direction times the first harmonic W_2 of the spatial modulation of the inversion. This latter contribution can be thought of as a reflection of the backward-running wave from the spatial inhomogeneity of the medium. The periodicity of the inhomogeneity leads to phase matching of the reflections with the forward-running wave as in one-dimensional Bragg reflection.[54] We can define separate coefficients for these two contributions:

$$\frac{\partial A_1}{\partial z} = -\beta_a^+ A_1 - \beta_r^+ A_{-1} ,$$
$$-\frac{\partial A_{-1}}{\partial z} = -\beta_a^- A_{-1} - \beta_r^- A_1 . \tag{45}$$

Experimentally, however, one does not distinguish β_a and β_r, but measures only the apparent attenuation of either wave. Using λ we can combine β_a and β_r into net effective attenuation coefficients for the two waves

$$\beta^+ \equiv \beta_a^+ - \lambda\beta_r^+, \quad \beta^- \equiv \beta_a^- - \lambda^{-1}\beta_r^- . \tag{46}$$

For stationary atoms the Fourier coefficients can be calculated analytically. We find

$$W_0 = \bar{W}/q_+ q_-,$$
$$W_2 = (q_+ - q_-)(q_+ + q_-)^{-1} W_0 , \tag{47}$$

where

$$q_\pm^2 = 1 + 2\alpha(1 \pm \lambda)^2 \cos^2\psi . \tag{48}$$

There is no velocity average, so we have immediately

$$\beta_a^+ = \beta_a^- = \frac{b^2 V(-\bar{W})}{c\gamma_2(1 - i\tan\psi)} \frac{1}{(q_+ q_-)} ,$$
$$\beta_r^+ = \beta_r^- = \left(\frac{q_+ - q_-}{q_+ + q_-}\right) \beta_a^+ . \tag{49}$$

The spatial inhomogeneity and the reflection coefficient vanish unless some standing-wave field is present ($\lambda > 0$). The equality of the coefficients for either running wave is a special property of the zero-velocity case and disappears when we calculate the effective attenuation coefficients:

$$\beta^+ = \frac{b^2 V(-\bar{W})}{c\gamma_2(1 - i\tan\psi)} \frac{1}{(q_+ + q_-)} \left(\frac{1+\lambda}{q_+} + \frac{1-\lambda}{q_-}\right), \tag{50}$$

$$\beta^- = \frac{b^2 V(-\bar{W})}{c\gamma_2(1 - i\tan\psi)} \frac{1}{(q_+ + q_-)} \frac{1}{\lambda} \left(\frac{1+\lambda}{q_+} - \frac{1-\lambda}{q_-}\right). \tag{51}$$

These agree with the results of Rautian or Kuznetsova.[55] Equations (50) and (51) can be converted into each other by changing λ to λ^{-1} with $q_\pm$ unchanged, that is, by exchanging the amplitudes of the two waves. This symmetry is merely a consequence of our original freedom to choose which wave we shall call forward running and which one backward.

As a function of detuning, the attenuation coefficient $\beta_a^\pm$ is approximately a Lorentzian resonance like (34), becoming weaker and broader at higher intensities. The reflection coefficient $\beta_r^\pm$ behaves more like the square of a Lorentzian and vanishes at low intensities. Since $\mathrm{Re}\beta_r^\pm$ is positive, the reflected wave is in phase with the oppositely running transmitted wave and increases its intensity. The increase is relatively greater for the weaker wave, that is, the weaker wave has a smaller effective attenuation coefficient. Just the reverse will be found for moving atoms in the Doppler limit. The effective attenuation coefficient of the stronger wave retains the qualitative character of β_a when the reflection coefficient is added by (46). But under some conditions ($\alpha > \frac{1}{2}$, and λ not too close to 1), the effective attenuation coefficient for the weaker wave has two symmetric peaks with a central minimum. This minimum arises from the reflection of the stronger wave and is not a Lamb dip.

B. Moving Atoms—Formal Solution

The case of moving atoms exposed to two running waves is more difficult since the moving atoms see opposite Doppler shifts for the two oppositely running waves and thus are effectively exposed to two different frequencies of excitation. Previous treatments[56–60] of atoms exposed to two nearly resonant frequencies ignored spatial dependence and considered the amplitude of one exciting wave to be very weak. Our treatment includes the spatial dependence for two running waves and arbitrary amplitudes.

If the two oppositely running waves had different frequencies in the laboratory frame, the moving atoms would still see just two frequencies of excitation. In fact, the solution for this case can be obtained from the results of this part simply by using the average frequency for our ω and shifting the Doppler weight function f_M to be centered at kv_z equal to one-half the difference of the two frequencies instead of zero. Thus no new information is obtained by using different frequencies for two oppositely running waves. The problem of two waves of different frequencies running in the same direction is quite different.[61]

The discussion of the stationary-atom case gives us the clue for solving the moving-atom case. When we introduce the two-running-wave form (38) for A into (14)–(16), we also introduce the Fourier expansions[62,63] (41) and (42) and a corresponding ex-

pansion for N.[64] Equating Fourier coefficients then leads to the following infinite set of coupled partial differential equations for the slowly varying amplitudes:

$$\left(\frac{\partial}{\partial t}+\vec{v}\cdot\nabla+inkv_z+\tfrac{1}{2}\gamma_a+\tfrac{1}{2}\gamma_b\right)N_n+\tfrac{1}{2}(\gamma_a-\gamma_b)W_n$$
$$=(\gamma_a N_a^0+\gamma_b N_b^0)\delta_{n0},\quad n \text{ even} \tag{52}$$

$$\left(\frac{\partial}{\partial t}+\vec{v}\cdot\nabla+inkv_z+\tfrac{1}{2}\gamma_a+\tfrac{1}{2}\gamma_b\right)W_n+\tfrac{1}{2}(\gamma_a-\gamma_b)N_n$$
$$=(\gamma_a N_a^0-\gamma_b N_b^0)\delta_{n0}-2ibM_{n+1}A_1^*-2ibM_{n-1}A_{-1}^*$$
$$+2ibM_{-n+1}^*A_1+2ibM_{-n-1}^*A_{-1},\quad n \text{ even} \tag{53}$$

$$\left(\frac{\partial}{\partial t}+\vec{v}\cdot\nabla+inkv_z+\gamma_2\right)M_n$$
$$=i(\omega-\omega_0)M_n-ibW_{n-1}A_1-ibW_{n+1}A_{-1},\quad n \text{ odd}. \tag{54}$$

Here δ_{n0} is a Kronecker δ arising from an assumption that the equilibrium populations N_a^0 and N_b^0 are not rapidly varying. The complexity of the problem lies in the $inkv_z$ terms, which differ for each Fourier component. Equations (52)–(54), together with the generalization of (44),

$$\left(\frac{\partial}{\partial t}+\gamma_c+c\frac{\partial}{\partial z}+\frac{c\nabla^2}{2ik}\right)A_1=ibV\int M_1 d^3v, \tag{55}$$

$$\left(\frac{\partial}{\partial t}+\gamma_c-c\frac{\partial}{\partial z}+\frac{c\nabla^2}{2ik}\right)A_{-1}=ibV\int M_{-1}d^3v, \tag{56}$$

form a complete set describing the three-dimensional time-dependent behavior of a two-level medium subject to two oppositely running waves. They can be solved approximately by truncating the Fourier expansions.

In this paper we consider only the one-dimensional plane-wave steady-state solution of (52)–(56). We therefore drop all derivatives with respect to time and the transverse coordinates. In (52)–(54) the $v_z\,\partial/\partial z$ terms will be much smaller than the ikv_z terms by the assumption of slow z variation in the Fourier coefficients (valid for $|\beta|\ll k$). We therefore also drop the z derivatives in (52)–(54) and similarly the second derivative in (55) and (56). The medium equations (52)–(54) are then algebraic coupled recursion relations for the Fourier coefficients. Their solution is expressible in terms of infinitely continued fractions, whose development is largely an exercise in condensing notation.

First we eliminate N_n by solving (52) and substituting into (53) to obtain

$$\gamma_1 W_n=p_n(\gamma_1\overline{W}f_M\delta_{n0}-2ibM_{n+1}A_1^*-2ibM_{n-1}A_{-1}^*$$
$$+2ibM_{-n+1}^*A_1+2ibM_{-n-1}^*A_{-1}),\quad n \text{ even} \tag{57}$$

where γ_1, $\overline{W}$, and f_M are defined by (25)–(27). The new dimensionless coefficient is

$$p_n=\frac{\gamma_a\gamma_b}{\gamma_a+\gamma_b}\left(\frac{1}{\gamma_a+inkv_z}+\frac{1}{\gamma_b+inkv_z}\right),\quad n \text{ even}. \tag{58}$$

Note that $p_0=1$. Next we solve (54) for M_n:

$$M_n=-i(b/\gamma_2)F_n^+(W_{n-1}A_1+W_{n+1}A_{-1}),\quad n \text{ odd}. \tag{59}$$

We have introduced

$$F_n^{\pm}=(1\mp i\tan\psi+iny)^{-1},\quad n \text{ odd} \tag{60}$$

where

$$y=kv_z/\gamma_2 \tag{61}$$

is our dimensionless velocity variable and $\tan\psi$ was defined by (35). Inserting (59) into (57) and expressing A_{-1} by (39) yields a three-term recursion for the W's alone:

$$(1+\alpha p_n S_n^+ +\alpha\lambda^2 p_n S_n^-)W_n-\alpha\lambda p_n R_{n+1}W_{n+2}$$
$$-\alpha\lambda p_n R_{n-1}W_{n-2}=\overline{W}f_M\delta_{n0},\quad n \text{ even} \tag{62}$$

where

$$R_n=F_n^+ +F_n^-,\quad n \text{ odd} \tag{63}$$

$$S_n^{\pm}=F_{n+1}^{\pm}+F_{n-1}^{\mp},\quad n \text{ even} \tag{64}$$

and α was defined by (24). Except for the indexing, R_n, p_n, and α are the same abbreviations as those used by Holt.[29]

The resonances implicit in p_n and F_n can be identified in perturbation theory with n-photon processes[44] involving absorption and emission of photons from the two running waves alternately. In strong fields these processes interfere to the extent that they cannot be distinguished and we make no attempt to distinguish them.

A continued-fraction solution can be developed directly from (62), but a more desirable form is obtained by first forming two coupled recursion relations. We temporarily define W_n for n odd by

$$W_n=W_{n-1}-W_{n+1},\quad n \text{ odd} \tag{65}$$

and try to remember that it is not a Fourier coefficient. Using (65) we eliminate $W_{n\pm2}$ from (62) to obtain

$$(1+\alpha p_n T_n)W_n+\alpha\lambda p_n R_{n+1}W_{n+1}-\alpha\lambda p_n R_{n-1}W_{n-1}$$
$$=\overline{W}f_M\delta_{n0},\quad n \text{ even} \tag{66}$$

where

$$T_n=S_n^+ +\lambda^2 S_n^- -\lambda R_{n+1}-\lambda R_{n-1}$$
$$=(1-\lambda)(S_n^+ -\lambda S_n^-),\quad n \text{ even}. \tag{67}$$

We now introduce the ratio of successive W's by letting

$$C_n = \alpha\lambda p_n R_{n+1} W_{n+1}/W_n \quad \text{for } n \geq 0, \text{ even} \tag{68}$$

and

$$C_n = W_{n+1}/W_n \quad \text{for } n > 0, \text{ odd.} \tag{69}$$

Then (65) becomes

$$C_{n-1} = \alpha\lambda p_{n-1} R_n/(1 + C_n), \quad n > 0, \text{ odd} \tag{70}$$

while (66) becomes

$$C_{n-1} = \alpha\lambda R_{n-1} p_n/(1 + \alpha p_n T_n + C_n), \quad n > 0, \text{ even.} \tag{71}$$

Equations (70) and (71) together are the desired recursion relations for a continued fraction with alternating structure. In particular we have

$$C_0 = \cfrac{\alpha\lambda p_0 R_1}{1 + \cfrac{\alpha\lambda R_1 p_2}{1 + \alpha p_2 T_2 + \cfrac{\alpha\lambda p_2 R_3}{1 + \cfrac{\alpha\lambda R_3 p_4}{1 + \alpha p_4 T_4 + \cdots}}}} . \tag{72}$$

The convergence of (72) is helped by the ny's in the coefficients p_n and R_n, but occurs even for $y = 0$. In the latter case (stationary atoms) all p's, R's, and T's are equal. The continued fraction becomes periodic[65] and can be evaluated analytically to recover the solution (47).

To complete the solution we must find a starting point for our recursion relations, namely, the inhomogeneous term occurring in (66) when $n = 0$. We use (68) to express W_1 in terms of C_0, and the definitions (65) and (63) to show that the W_{-1} term is the complex conjugate of the W_1 term. Then (66) with $n = 0$ has the solution

$$W_0 = \frac{\overline{W} f_M}{1 + \alpha T_0 + 2\,\mathrm{Re}\, C_0} , \tag{73}$$

where C_0 is given by (72). All other W_n may now be obtained recursively from W_0 and (68)–(71), for example,

$$W_2 = C_1(1 + C_1)^{-1} W_0 . \tag{74}$$

Finally the attenuation and reflection coefficients are obtained by inserting (59) into (44). Comparing the results with (45), we find

$$\beta_a^{\pm} = -(b^2 V/c\gamma_2) \int F_{\pm 1}^{+} W_0\, d^3v , \tag{75}$$

$$\beta_r^{\pm} = -(b^2 V/c\gamma_2) \int F_{\pm 1}^{+} W_{\pm 2}\, d^3v . \tag{76}$$

Converting the integration variable to y, we can combine the constants into the unsaturated attenuation coefficient at resonance (31) to find

$$\beta_a^{+} = \frac{\beta_0}{\pi} \int \frac{F_1^{+} e^{-\eta^2 y^2} dy}{1 + \alpha T_0 + 2\,\mathrm{Re} C_0} \tag{77}$$

and similar expressions for the other coefficients. Here $\eta = \gamma_2/ku$ is a measure of the ratio of homogeneous to inhomogeneous broadening. For large η, replacing the exponential by $\pi^{1/2}\eta^{-1}\delta(y)$ recovers the solutions of Sec. IV A. For small η, replacing the exponential by unity yields the Doppler limit. The coefficients obey the symmetry

$$\beta_{a,r}^{\mp}(\alpha, \lambda, \tan\psi) = \beta_{a,r}^{\pm}(\alpha\lambda^2, \lambda^{-1}, \tan\psi) \tag{78}$$

associated with the invariance of the problem to which direction in z is called forward. Equations (70)–(78) together with the definitions (58), (60), (61), (63), (64), and (67) comprise our formal solution for the attenuation of two oppositely running waves by moving atoms.

C. Connection with Laser Theory

The theory of laser oscillators has most commonly been built on the assumption of small gain per pass and high-Q cavities, even though these conditions are not always satisfied experimentally. One then considers spatially fixed eigenmodes of the optical cavity being amplified or attenuated in time, rather than running waves varying in space.

We write the field amplitude as a sum of time-dependent amplitudes for each spatial mode:

$$A(\vec{r}, t) = \sum_i A_i(t)\, u_i(\vec{r}) . \tag{79}$$

The mode functions are defined by

$$(c^2\nabla^2 + \omega_i^2)\, u_i(\vec{r}) = 0 \tag{80}$$

and appropriate boundary conditions. We shall assume they are orthogonal and normalized to the volume V:

$$\int u_i(\vec{r})\, u_j^*(\vec{r})\, d^3r = V\delta_{ij} . \tag{81}$$

Using (79)–(81) in (13) we find an equation for the amplitude of each mode

$$\left(\frac{\partial}{\partial t} + \gamma_i - i\omega + i\omega_i\right) A_i = \tfrac{1}{2} i\omega\chi_i A_i , \tag{82}$$

where we have assumed $\omega \simeq \omega_i$. The γ_i include now not only any conductive losses of the medium, but also losses at the boundaries, which may differ for different modes. The susceptibility for the ith mode appearing in (82) is defined by

$$\chi_i A_i = (2b/\omega) \int\int M(\vec{r}, \vec{v}, t)\, u_i^*(\vec{r})\, d^3r\, d^3v . \tag{83}$$

Since (14)–(16) are nonlinear, they do not decompose neatly into modes, but lead to coupling between the different modes.[10] Thus χ_i will in general depend on the amplitudes of all excited modes

and (82) must be considered to be a coupled set of equations.

Let χ_i' and χ_i'' be the real and imaginary parts of χ_i. Then in steady-state oscillation, (82) says that the frequency of the ith mode is determined by the real part of the susceptibility satisfying

$$\omega_i - \omega = \tfrac{1}{2}\omega\chi_i' . \tag{84}$$

The amplitude of the mode is determined by the imaginary part of the susceptibility obeying

$$-\chi_i'' = 2\gamma_i/\omega_i \equiv 1/Q_i , \tag{85}$$

where Q_i is the quality factor of the cavity for that mode. These are the self-consistency requirements of laser theory.[10,66]

To utilize the general solution of Sec. IV B, consider an idealized ring laser with two eigenmodes corresponding to forward- and backward-running plane waves

$$u_1(\vec{r}) = e^{ikz}, \quad u_{-1}(\vec{r}) = e^{-ikz} . \tag{86}$$

Inserting these mode functions in (83) and comparing with (44)–(46), we find the susceptibility is directly related to the effective attenuation coefficients

$$\chi_{\pm 1} = (2ic/\omega)\,\beta^{\pm} . \tag{87}$$

Note that the reflection-coefficient part of β will appear in (82) as a term coupling the two running waves, but arising solely from the nonlinear properties of the medium. Similar coupling terms attributed to optical properties of the cavity have been introduced in ring-laser theory[67] to account for the observed mode coupling properties. The results of Sec. IV B, together with (87) and (82), provide a complete formal solution for the high-intensity ring laser. Previous analyses of ring lasers[68–70] have been done by perturbation theory, except for a recent analysis by Takata,[71] who formulates the ring-laser problem for arbitrary intensities but then looks at special cases without developing the continued fraction.

Now consider the more conventional standing-wave laser. A plane standing-wave mode function normalized by (81) is

$$u_{sw} = \sqrt{2}\,\sin kz . \tag{88}$$

Expanding the sine function in exponentials, we find that the standing-wave problem is obtained from the preceding ring-laser formulation simply by setting $A_1 = -A_{-1} = A_{sw}/\sqrt{2}\,i$ and equating the frequencies ω_i and losses γ_i. That is, (82) holds where the standing-wave susceptibility is

$$\chi_{sw} = (2ic/\omega)\beta^{+} , \tag{89}$$

with β^{+} evaluated for $\lambda = 1$ and $\alpha = b^2\,|A_{sw}|^2/\gamma_1\gamma_2$. Specifically, the analog of (77) is

$$\chi_{sw} = \frac{i\chi_0''}{\pi}\int \frac{F_1^{+}(1+C_1)^{-1}e^{-\eta^2 y^2}\,dy}{1+2\,\mathrm{Re}C_0} , \tag{90}$$

where $\chi_0'' = (2c/\omega)\beta_0$ is the imaginary part of the unsaturated susceptibility at resonance. The imaginary part of (90) simplifies further to

$$\chi_{sw}'' = \frac{\chi_0''}{\pi}\int \frac{\mathrm{Re}C_0\,e^{-\eta^2 y^2}\,dy}{2\alpha(1+2\,\mathrm{Re}C_0)} . \tag{91}$$

Note that for standing waves ($\lambda = 1$), the symmetry (78) tells us $\beta^{+} = \beta^{-}$ and (67) tells us that all the T_n's vanish, improving the symmetry of the continued fraction (72) for C_0. The results (84), (85), and (91) are equivalent to the solutions previously found for high-intensity gas lasers.[27–29]

When an absorption cell is placed within the cavity of a gas laser,[11,12] the behavior of the laser can still be described by (82), where the susceptibility is now the sum of susceptibilities for the absorbing and amplifying media. Such an analysis has been carried out in various approximations[72–75] and will not be treated here. If the internal absorption cell leads to passive Q switching or mode locking of the laser, the analysis is best done by the concept of running-wave pulses rather than cavity modes.[63,76,77]

D. Perturbation Solution

Lamb originally solved the laser problem by iterating the nonlinear equations of motion to obtain the polarization as a power series in the field amplitude. We could do the same starting with (52)–(54). However, the result is more readily obtained by expanding the continued fractions of the general solution in powers of α.

From (73), (72), and (67), we find to first order in α

$$\begin{aligned} W_0 &= \bar{W} f_M(1 - \alpha T_0 - 2\,\mathrm{Re}\,\alpha\lambda R_1) \\ &= \bar{W} f_M(1 - \alpha S_0^{+} - \alpha' S_0^{-}), \end{aligned} \tag{92}$$

where $\alpha' \equiv \lambda^2\alpha$ is proportional to the intensity of the backward wave. The $S_0^{\pm}$ are Lorentzians centered at $\omega = \omega_0 \pm kv_z$ and represent the Bennett holes burned in the inversion W_0 by each of the two running waves. For running waves of different amplitude the holes are of different depth. We introduce the approximation (92) into (75) and evaluate the y integral in the Doppler limit by contour integration to find

$$\beta_a^{+} = \beta_0(1 - \alpha - \alpha'\cos\psi\, e^{i\psi}) . \tag{93}$$

Recalling the definition of ψ (35), we note that

$$\cos^2\psi = \gamma_2^2/[\gamma_2^2 + (\omega - \omega_0)^2] . \tag{94}$$

Thus the real part of (93) has a Lorentzian dip in it centered at the atomic resonance frequency with

the homogeneous linewidth γ_2 and depth proportional to the intensity α' of the oppositely running wave. This dip arises from the additional atomic saturation when both running waves interact with the same atoms, rather than with atoms of different velocities, that is, when the two Bennett holes overlap. It is the analog in absorption of the Lamb dip in gas-laser emission. Inserting (93) for β^+ in (89) and then solving (85) for α, one recovers Lamb's third-order solution for the gas laser in the Doppler limit. The dispersive (imaginary) part of (93) also has structure of width γ_2 in addition to the structure of width ku given in (36) and neglected in the Doppler limit.

From the symmetry (78) we find

$$\beta_a^- = \beta_0(1-\alpha'-\alpha\cos\psi\, e^{i\psi}). \tag{95}$$

The two attenuation coefficients have the same form, but the dip is relatively larger in the attenuation coefficient of the weaker running wave. This qualitative result continues to hold when α and α' are too large for these perturbation solutions to be valid. Henceforth, we shall define the forward-running wave as the wave of greater amplitude ($\alpha \geq \alpha'$ or $\lambda \leq 1$) and concentrate on the attenuation of the backward wave.

In the experiments of Hänsch *et al.*[23,78] and Bordé[16] the change in attenuation of the weaker wave is observed as the stronger wave is switched on and off. Their difference signal then will be proportional to

$$S = \alpha' \mathrm{Re}[\beta^-(\alpha=0) - \beta^-(\alpha>0)]\ . \tag{96}$$

From the approximation (95) for β^- we find

$$S = \alpha\alpha'\beta_0\cos^2\psi\ , \tag{97}$$

a simple Lorentzian line whose strength is proportional to the product of the intensities of the two running waves.

We neglected the reflection coefficients above since they are of higher order. From (74) and (71) we obtain

$$W_2 = (\alpha\lambda R_1 p_2 + O\alpha^2)W_0\ .$$

In the Doppler limit the leading term vanishes upon integration over y, since all factors F_1^+, R_1, and p_2 in (76) have poles in the upper half-plane, while the integration contour may be closed around the lower half-plane. If the Doppler limit is not taken, this term can be evaluated in terms of differences of Z functions[79] and will be of order $\eta\alpha$. A larger contribution may come from second-order terms in α. The F_{-1} components of S_0 appearing in W_0(92) then have poles in the lower half-plane and give

$$\beta_Y^+ = -\tfrac{1}{4}\gamma_1\alpha\lambda\beta_0[\alpha(B_a+B_b)+\alpha'(B_a^*+B_b^*)/(1-i\tan\psi)], \tag{98}$$

where

$$B_a = (2+i\tan\psi)(1+i\tan\psi)^{-1}(2+\gamma_a+2i\tan\psi)^{-1}$$

and B_b is obtained by replacing γ_a by γ_b. The γ_i are the population relaxation rates normalized to the homogeneous linewidth,

$$\gamma_i = \gamma_i/\gamma_2, \quad i = a, b, 1. \tag{99}$$

The real part of β_Y^+ is a negative resonance function, narrower than the Lorentzian (94), and sometimes becoming positive before vanishing at large detuning.

If we expand (77) to second order in α, combine with (98), and apply the symmetry (78), we find the complete second-order result

$$\mathrm{Re}\beta^- = \beta_0[1-g(\alpha') - \alpha f(\alpha, \alpha', \tan\psi)], \tag{100}$$

where

$$g(\alpha') = \alpha' - \tfrac{3}{2}\alpha'^2, \tag{101}$$

$$f(\alpha,\alpha',\tan\psi) = \cos^2\psi[1 - \alpha F(\tan\psi) - \alpha' G(\tan\psi)], \tag{102}$$

$$F(\tan\psi) = \tfrac{1}{2}(1+2\cos^2\psi) + \tfrac{1}{2}\gamma_1(F_a/D_a + F_b/D_b), \tag{103}$$

$$G(\tan\psi) = 1 + 2\cos^2\psi + \tfrac{1}{2}\gamma_1(G_a/D_a + G_b/D_b), \tag{104}$$

$$F_a = -1 - \cos^2\psi + (4+\gamma_a)\cos^4\psi\ , \tag{105}$$

$$G_a = (-1+\gamma_a) + (3+\gamma_a)\cos^2\psi + (4+\gamma_a)\cos^4\psi, \tag{106}$$

$$D_a = 4 + \gamma_a(4+\gamma_a)\cos^2\psi, \tag{107}$$

with similar expressions for F_b, G_b, and D_b using γ_b. We have used this solution to calculate the standing-wave laser susceptibility for $\gamma_a + \gamma_b = 2$ and find agreement with the fifth-order perturbation calculation of Uehara and Shimoda.[80]

We have introduced f in (100) since the difference signal (96) is proportional to it:

$$S = \alpha\alpha'\beta_0 f(\alpha,\alpha',\tan\psi)\ . \tag{108}$$

The effect of the F and G terms in (102) is to make the signal weaker, broader, and not exactly Lorentzian. Most easily measured is the broadening. We find the half-width at half-height

$$\tan\psi_{1/2} = 1 + \kappa\alpha + \kappa'\alpha' + O\alpha^2, \tag{109}$$

where

$$\kappa = F(0) - F(1) = \tfrac{1}{2} + \tfrac{1}{2}\gamma_1(C_a + C_b), \tag{110}$$

$$\kappa' = G(0) - G(1) = 1 + \tfrac{1}{2}\gamma_1(C_a' + C_b'), \tag{111}$$

$$C_a = \frac{1}{2+\gamma_a} + \frac{2-\gamma_a}{16+8\gamma_a+2\gamma_a^2}, \tag{112}$$

$$C_a' = \frac{3}{2+\gamma_a} - \frac{6+7\gamma_a}{16+8\gamma_a+2\gamma_a^2}, \tag{113}$$

and similarly for C_b and C_b'. Since $\kappa' > \kappa$, a running wave is more effective in power broadening the dip in its own attenuation than is the oppositely running wave; that is, β^+ has a broader dip than β^-. The broadening is greatest for equal relaxation rates ($r_a = r_b = r_1 = 1$) for which $\kappa = 34/39$ and $\kappa' = \frac{3}{2}$. The numerical calculations described in Sec. IV G confirm these values of κ and κ' for α, $\alpha' \leq 0.1$, but give much less broadening than (109) at higher powers.

The power-series solution is useful only for quite small values of α and α'. By setting α equal to zero, we can find the self-saturation function g exactly from the solution (37) for a single running wave

$$g(\alpha') = 1 - (1 + 2\alpha')^{-1/2} . \tag{114}$$

Thus the power series cannot converge for $\alpha' > \frac{1}{2}$. We shall see in Sec. IV F that the radius of convergence may be even smaller. Holt[29] has found the power series to be useful in laser theory only for α up to 0.05 and our numerical calculations tend to support this. Nevertheless, Tatarenkov *et al.*[81] analytically determined the power broadening of the susceptibility in second order, while Shimoda and Uehara[82] have extended laser theory to even higher order in α.

E. Solution for One Wave Very Weak

Several experimenters[16,21,78,83] have recently been using a strong forward-running wave (saturating beam) and a weak backward-running wave (probe beam). This suggests that a power-series solution in the amplitude ratio λ would be of interest. We here find the lowest-order contributions to such a solution.

In the limit of small λ the inversion density is

$$W_0 = \bar{W} f_M / (1 + \alpha S_0^+) . \tag{115}$$

Only one of the Bennett holes is appreciable. Inserting (115) into (75) we find β_a^+ in the Doppler limit to be the same as (37) for a single running wave with corrections of order λ^2. The tuning dip has gone to zero with λ. For the weak wave, however, the tuning dip approaches a finite limit:

$$\beta_a^- = \beta_0 \left(1 - \frac{Q^2 - 1}{Q(Q + 1 - 2i\tan\psi)}\right), \tag{116}$$

where $Q = (1 + 2\alpha)^{1/2}$. The real part of this result has been obtained previously.[83] The signal (96) becomes

$$S = \alpha' \beta_0 (1 - Q^{-1}) \mathcal{L} , \tag{117}$$

where $\mathcal{L}$ is a power-broadened Lorentzian function

$$\mathcal{L} = [1 + 4\tan^2\psi/(1 + Q)^2]^{-1} . \tag{118}$$

Note that the width of the Lorentzian is not the width $Q\gamma_2$ of the Bennett hole in (115), but an average of that with the unsaturated interaction width γ_2 of the probe beam.

Since W_2 is proportional to C_1 and hence to λ, the reflection coefficients $\beta_r^\pm$ are of order λ. From (46), β_r^+ then makes a contribution of order λ^2 to β^+. However, β_r^- is divided by λ in (46) and makes a finite contribution to β^- in the small λ limit. This possibility was overlooked by Basov *et al.*[83] From (74), (71), (73), and (76) we find

$$\beta_r^- = \frac{\beta_0}{\pi} \int \frac{F_{-1}^+ (\alpha\lambda R_{-1} p_{-2}) e^{-\eta^2 y^2} dy}{(1 + \alpha p_{-2} S_{-2}^+)(1 + \alpha S_0^+)} + O\lambda^2 . \tag{119}$$

In the Doppler limit the integral can be evaluated by contour integration around the sole pole in the upper half-plane at $y = \tan\psi + iQ$ (arising from $1 + \alpha S_0^+$). The result is

$$\beta_r^- = \frac{-\alpha\lambda r_1 \beta_0 (Q - 1) h_3 (h_1 + i\tan\psi)(h_a + h_b)}{Q h_1 [h_1 h_3 h_a h_b + \frac{1}{2}\alpha r_1 (h_1 + h_3)(h_a + h_b)]}, \tag{120}$$

where

$$h_1 = 1 + Q - 2i\tan\psi, \quad h_a = r_a + 2Q - 2i\tan\psi,$$
$$h_3 = 1 + 3Q - 2i\tan\psi, \quad h_b = r_b + 2Q - 2i\tan\psi.$$

The denominator has $Q - i\tan\psi$ as a factor. Just like the perturbation result (98), the real part of (120) is a negative resonance function becoming positive before vanishing at large detuning. Combined with (116) it effectively increases the attenuation, reduces the signal strength, and increases its width.

The reduction in strength of the signal due to reflection is found by evaluating (116) and (120) at resonance:

$$S(\tan\psi = 0) = \alpha' \beta_0 \frac{Q - 1}{Q} \left(1 - \frac{r_1 (Q^2 - 1)(3Q + 1)(4Q + r_a + r_b)}{4QH}\right), \tag{121}$$

where

$$H = (3Q + 1)(Q + 1)(2Q + r_a + r_b) + r_1 (Q^2 - 1) \times (2Q + 1) + r_a r_b (Q + 1)^2 .$$

For small α we recover the perturbation intensity (97). As α increases, the signal intensity slowly approaches a finite limit, which we can find by assuming Q is large[84]:

$$S(\tan\psi = 0) \sim \alpha' \beta_0 [1 - 3r_1/(6 + 2r_1)] . \tag{122}$$

For equal relaxation rates ($r_1 = 1$), the reflection part reduces the signal by up to $\frac{3}{8}$, a significant contribution. At $\alpha = 2$ the reduction is about 20%. This reduction results in an apparent increase in width (26% at $\alpha = 2$). In the same limit as (122), β_a^-

becomes small, while β_r^- does not, so that the major contribution to the attenuation of the weak wave is destructive interference by the reflection of the stronger wave.

Recently results equivalent to (116) and (120) have been calculated independently.[43,44] These authors give special attention to the high-power case, relating some of their results to the Autler–Townes dynamic Stark effect.[85] In the rest frame of an atom moving with axial velocity v_z, a very strong field at the Doppler-shifted frequency $\omega - kv_z$ drives the atom to make successive transitions at the Rabi flipping frequency $2p = [(\omega - kv_z - \omega_0)^2 + 4b^2 |A_1|^2]^{1/2}$. This results in modulation of the inversion density or the introduction of sidebands on the polarization. The oppositely running weak wave at the Doppler-shifted frequency $\omega + kv$ will resonate with these sidebands if $\omega + kv_z = \omega - kv_z \pm 2p$. These resonances can be found in the factor $(1 + \alpha p_{-2} S_{-2}^+)$ of the integrand of (119) by neglecting the relaxation rates.

Haroche and Hartmann[44] also point out that at high powers the integrand for β^- may become negative at small velocities (but not at zero velocity). In other words, the reflection of the strong wave is so intense that atoms of certain velocities effectively amplify the weak beam, although their populations are not inverted. Our numerical calculations discussed in Sec. IV G confirm this phenomenon at $\alpha = 4$ with λ values as large as 0.7. The attenuation by atoms of other velocities will usually mask the amplification by a few atoms when the velocity integration is performed. However, Haroche and Hartmann obtain a net negative value for β^- with the parameters $\alpha = 50$, $\lambda = 0$, $|\tan\psi| < 6$, and $\eta = 0.45$ for which the saturation width of the Bennett hole exceeds the Doppler width.

F. Rate-Equation Approximation

The rate-equation approximation was first suggested by Lamb (Sec. 19 of Ref. 10), but he did not investigate its validity. Greenstein[66] used it in his extensive analysis of the gas laser, as did Balazs and Tobias.[41] Subsequently it was related to the high-intensity laser theory and received its name.[27] Holt[29] has compared it numerically with better approximations.

The rate-equation approximation has been described[66] as the neglect of population pulsations seen by individual atoms. (The beat between the two Doppler-shifted frequencies seen by a moving atom modulates its transition probability). In our macroscopic theory it can equivalently be described as the neglect of the spatial modulation of the population inversion, that is, we replace the Fourier series (42) by its constant term W_0. In the coupled equations (52)–(54) we retain only W_0, M_1, and M_{-1}. Although we thereby omit some terms of fairly low order in perturbation theory, the three remaining equations include the more important parts of the interaction to all orders and provide an approximation vastly superior to truncating a poorly converging power series.

Neglecting the spatial modulation in our general solution means first of all that we are neglecting the reflection coefficients entirely. To calculate the attenuation coefficients, we note from (57) that W_n will vanish if we set $p_n = 0$ for $n \neq 0$. Doing this in (72) gives us $C_0 = \alpha\lambda R_1$, the lowest-order truncation of our continued fraction. We then find from (73)

$$W_0 = \bar{W} f_M / (1 + \alpha S_0^+ + \alpha' S_0^-) , \tag{123}$$

which, like (92), includes both Bennett holes. The integrals (75) can be evaluated in the Doppler limit by contour integration or partial fractions. The poles are roots of a fourth-order polynomial. Using the algebraic solution for a quartic,[86] we can express the result by the following sequence of definitions:

$$\Lambda = 2 - \sec^2\psi + \alpha + \alpha' , \tag{124}$$

$$R^2 = \sec^2\psi(\sec^2\psi + 2\alpha + 2\alpha') , \tag{125}$$

$$\epsilon = (\alpha - \alpha')\tan\psi , \tag{126}$$

$$A_m = \tfrac{1}{6}(3R^2 + \Lambda^2)^{1/2} , \tag{127}$$

$$C_m = [\Lambda(\Lambda^2 - 9R^2) + 27\epsilon^2]/216 , \tag{128}$$

$$\phi = \cos^{-1}(C_m / A_m^3) , \tag{129}$$

$$U^2 = 2A_m \cos(\tfrac{1}{3}\phi) - \tfrac{1}{3}\Lambda , \tag{130}$$

$$X^2 = U^2 + \Lambda + \epsilon/U , \tag{131}$$

$$Y^2 = U^2 + \Lambda - \epsilon/U , \tag{132}$$

$$\beta_\alpha^\pm = \frac{\beta_0[(X+Y)(1 - i\tan\psi) \pm i\,U(X-Y)]\,[(1 + i\tan\psi)^2 + U^2 + XY]}{XY[4U^2 + (X+Y)^2]} . \tag{133}$$

Here (124)–(126) define the coefficients of the quartic $y^4 + 2\Lambda y^2 + 4\epsilon y + R^2$, (127)–(130) are the trigonometric solution for the resolvent cubic associated with the quartic, and the roots of the quartic are $U \pm iX$ and $-U \pm iY$.

The solution (133) simplifies in the following special cases. When the applied field is in exact resonance with the atoms ($\tan\psi = 0$), we have

$$\beta_a^{\pm} = \beta_0(1+2\alpha+2\alpha')^{-1/2} . \quad (134)$$

The equality of the two attenuation coefficients here is a property of the rate-equation approximation and is not true when reflections are included. Note also that the power-series expansion of (134) converges only when $\alpha+\alpha'<\frac{1}{2}$, a more severe restriction than that found in Sec. IV D. When the two running waves are of equal amplitude ($\alpha = \alpha'$), we have

$$\beta_a^{\pm} = \beta_0 \frac{[(1+i\tan\psi)^2+R]\ (1-i\tan\psi)}{R[2(R+\Lambda)]^{1/2}} . \quad (135)$$

The imaginary part of the standing-wave susceptibility obtained from (135) and (89) is the result of Greenstein.[66] When the applied field is off resonance much more than the homogeneous width ($\tan\psi \gg Q$), we have

$$\beta_a^{+} = \beta_0(1+2\alpha)^{-1/2}, \quad \beta_a^{-} = \beta_0(1+2\alpha')^{-1/2}. \quad (136)$$

In this case the two running waves interact with different velocity groups of atoms and are attenuated independently as though the other wave were not present [cf. (37)]. Finally when α' goes to zero we recover the solutions (37) and (116) of the preceding part.

As an analytic solution, (124)–(133) are so complex as to be useless, particularly since X and Y may be undefined (U and ϵ both vanish) for the special cases $\tan\psi = 0$ or $\alpha = \alpha'$. However, (124)–(133) are readily evaluated by computer. As a function of detuning, the Doppler-limit attenuation coefficients are flat with a saturation dip at the center. The depth of the dip is proportional to the difference signal (96) evaluated at resonance:

$$S(\tan\psi = 0) = \alpha'\beta_0[(1+2\alpha')^{-1/2} - (1+2\alpha+2\alpha')^{-1/2}] . \quad (137)$$

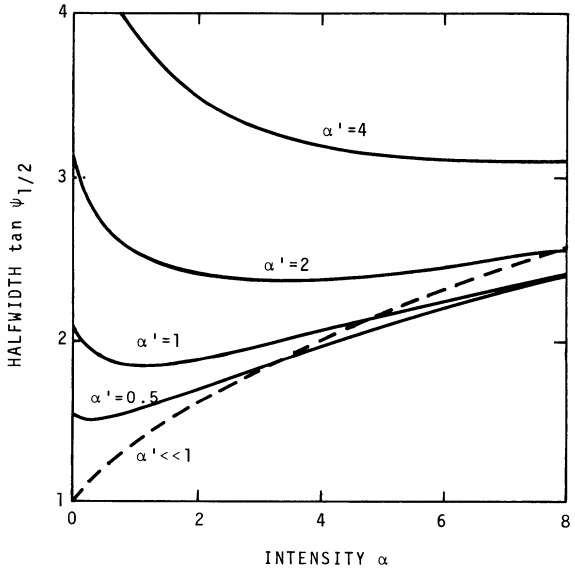

FIG. 1. Power broadening of dip in attenuation coefficients as a function of the dimensionless intensity α of one running wave for various intensities α' of the oppositely running wave. Rate-equation approximation in the Doppler limit.

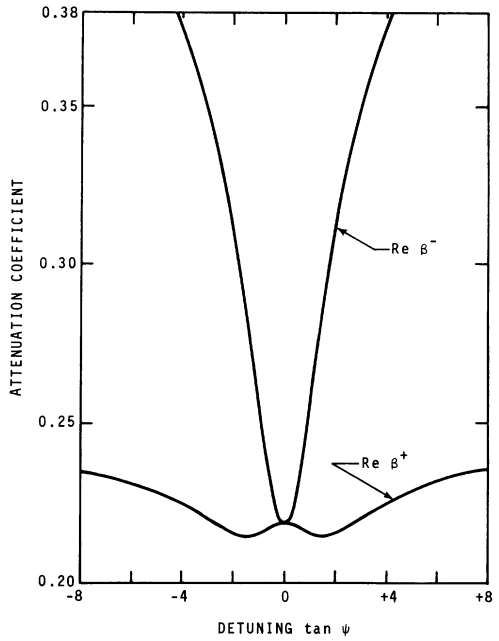

FIG. 2. Line shapes for real parts of Doppler-limit attenuation coefficients in the rate-equation approximation. The shallow dip in the attenuation coefficient Reβ^+ for the stronger wave shows the line-splitting effect. The much deeper dip in the attenuation coefficient Reβ^- for the weaker wave is shown for comparison. The intensities α and α' of the two running waves are 8 and 2, respectively.

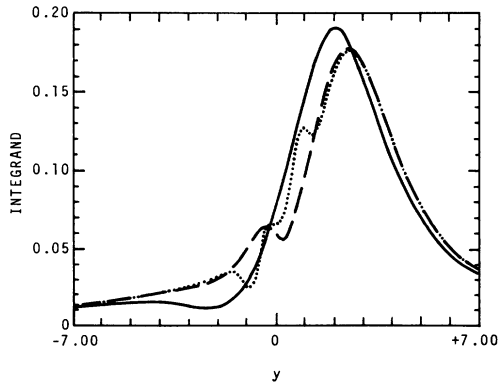

FIG. 3. Integrand for an effective attenuation coefficient in the Doppler limit as a function of dimensionless velocity y. The solid curve is the rate-equation approximation; the dashed curve is truncation case A; and the dotted curve is truncation case 1 (most accurate). The intensities α and α' of the two waves are both 2 and the detuning $\tan\psi$ is 2.

The relative depth is greater if the backward-wave intensity α' is weak. The power broadening of the dip, obtained numerically, is shown in Fig. 1. The width at half-height is not a monotonic function of α and α' as the perturbation result (109) is, because of the changing depth and hence changing level at which the width is measured. For fixed detuning, the attenuation coefficients do decrease monotonically as α or α' is increased.

The shape of the saturation dip can be well fitted by a Lorentzian in most cases. However, when α is large and α' appreciably smaller, the dip in β_a^+ splits. This effect arises solely from the nonlinearity of the overlap of the two Bennett holes in (123). To treat it analytically we make a first-order expansion in α':

$$\mathrm{Re}\beta_a^+ = \frac{\beta_0}{2\pi}\int \frac{S_0^+}{1+\alpha S_0^+}\left(1-\frac{\alpha' S_0^-}{1+\alpha S_0^+}\right)dy$$

$$= (\beta_0/Q)\,(1-\alpha' K), \tag{138}$$

where

$$K(\alpha, \tan\psi) = \frac{(2Q^2-Q+1)\mathfrak{L} - 2Q(Q-1)\mathfrak{L}^2}{Q^2(Q+1)} \tag{139}$$

and $\mathfrak{L}$ was defined in (118). For large α the Lorentzian S_0^- is relatively narrow and can be envisioned as a δ function reproducing the remainder of the integrand. Equation (139) shows a dip that splits when α exceeds $(5+3\sqrt{17})/16 = 1.09$, but larger α values are required for a significant effect. In the high-power limit we have $K \sim 2\mathfrak{L} \times(1-\mathfrak{L})/Q$, that is, the two components reach a separation comparable to their width while their amplitudes diminish. Figure 2 shows an example of a split line shape for β_a^+ at a high-power level. For comparison the much deeper dip in β_a^- is also shown. However, when the attenuation coefficients are multiplied by the powers in the respective beams, the signal powers are more nearly comparable.

The validity of the rate-equation approximation depends on the importance of the neglected coefficients p_n. The p_n are complex resonance functions centered at $y=0$ with a width of the order of the smaller of r_a, r_b divided by n. Their effect on $M_{\pm 1}(y)$ is to add an extra wiggle about $y=0$, but in such a way that the changes in area tend to compensate when the integration over y is performed (see Fig. 3). This compensation is better when the wiggle is narrower, so the approximation should be good for either r_a or r_b small. This conclusion is reinforced by the contour-integration method, in which we evaluate p_{-n} at poles like $y=\tan\psi + iQ$ obtaining factors like $r_1/(nQ+r_a - in\tan\psi)$. In the approximate solutions (100)–(107) and (120) the terms arising from $p_{\pm 2}$ are those with factor r_1, which is less than twice the smaller of r_a and r_b. Also in (71) and (72) p_2 occurs multiplied by R_1, which peaks at $y=\tan\psi$, so the product is small for large detuning. Thus the rate-equation approximation is good in two cases: highly unequal relaxation rates and large detuning. It is also valid, of course, at low powers when the coefficient $\alpha\lambda$ of p_2 is small.

G. Numerical Evaluation in the Doppler Limit

Better approximations than the preceding are found by truncating the continued fraction further out. This is equivalent to truncating the system (52)–(54) or the Fourier series (41) and (42). Physically we are neglecting the higher-order

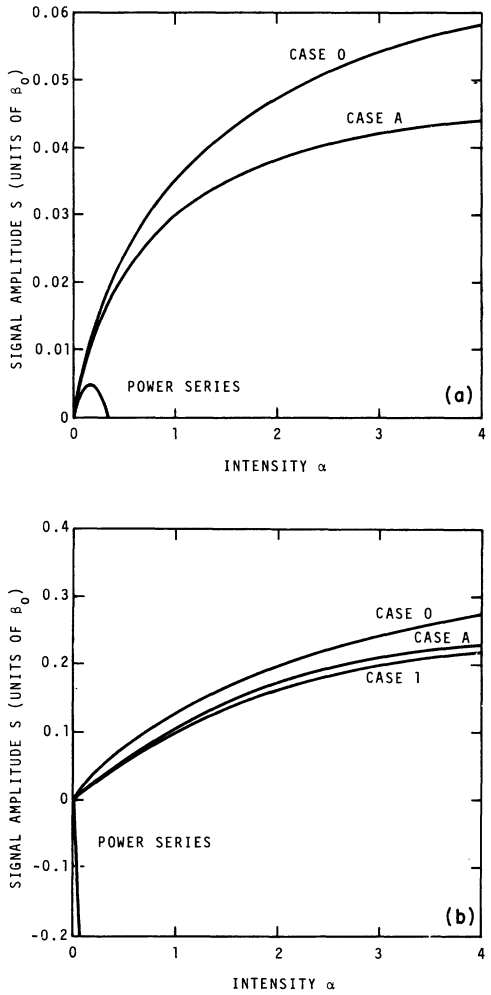

FIG. 4. Signal amplitude at resonance in the Doppler limit as a function of saturating beam intensity α for the three lowest-order truncation cases and the second-order power series. Probe beam intensities α' are 0.1 for (a) and 1.0 for (b). In (a) case 1 practically coincides with case A.

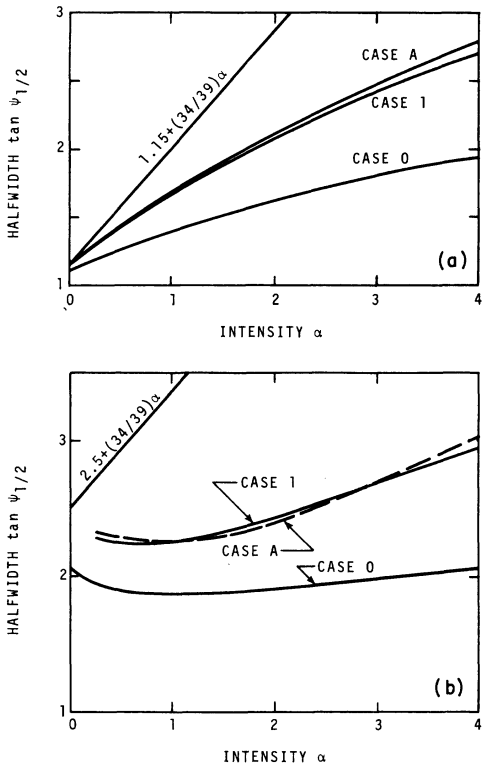

FIG. 5. Power broadening of saturated absorption signal as a function of saturating beam intensity α for the three lowest-order truncation cases in the Doppler limit. The straight line is the second-order power-series result (109). Probe beam intensities α' are 0.1 for (a) and 1.0 for (b).

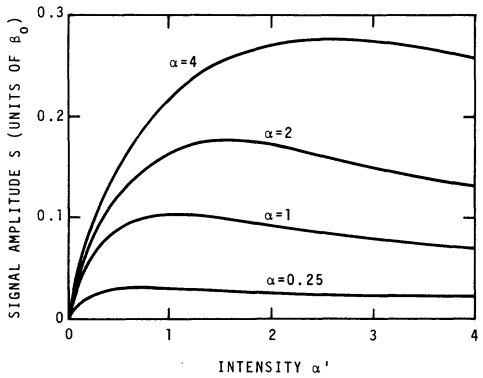

FIG. 6. Signal amplitude at resonance in the Doppler limit as a function of probe beam intensity α' for various saturating beam intensities α.

multiphoton processes. The lowest-order nontrivial truncation, which arises by setting p_2 equal to 0, was discussed in Sec. IV G. The next lowest truncation is Holt's case A,[29] in which we retain p_2 but set $F_3^{\pm}=0$.[87] It is equivalent to retaining the variables W_0, $M_{\pm1}$, and $W_{\pm2}$ and is the simplest case giving a value for the reflection coefficient. We can obtain Holt's cases B and C by setting $F_5^{\pm}$ and $F_7^{\pm}$, respectively, equal to zero. We can also form intermediate cases by setting p_4 or p_6 to zero. We refer to these as cases 1 and 2, respectively (case 0 would be the rate-equation approximation). Fleck's results [Ref. 63, Eq. (27)] correspond to case 1 for stationary atoms. The reflection coefficient for small λ (119) also corresponds to case 1 but changes very little in case A (drop F_3^- from S_{-2}^+).

The higher-order truncation cases are too complex to integrate analytically. To see what is involved for numerical integration a representative sample of the integrand for β^- in the Doppler limit is shown in Fig. 3 for the three lowest-order truncation cases. The rate-equation approximation gives a smooth peak centered at $y=\tan\psi$. Case A has a superposed wiggle about $y=0$ arising from p_2 and slightly shifting the peak. Case 1 has additional narrower wiggles about $y=\pm\frac{1}{3}\tan\psi$ arising from R_3 and T_2. The presence of these wiggles requires a closer spacing of sample points for numerical integration. On the other hand, the difference in the area under a wiggle and under the smooth curve of a lower-order truncation is small. Thus when the curves shown in Fig. 3 are integrated, case A differs from the rate-equation approximation by 1.6% and from case 1 by only 0.8%, even though the integrand values differ by a factor of 2 at $y=-1$. Because of this compensation effect, noted by Holt,[29] truncation of the Fourier series is a much better approximation than one would estimate from the convergence of the continued fraction. None of the calculations reported here go beyond case B. Lower-order truncation cases are satisfactory for small α values, large detuning, or for β^+ when it differs appreciably from β^-.

A computer program was developed to evaluate the truncated continued fractions and then perform the velocity integration to obtain the real parts of $\beta^{\pm}$. (The imaginary parts have not been studied numerically.) The long Lorentzian tails of the Doppler-limit integrand are split off and integrated separately with respect to a reciprocal variable, thus reducing the number of integrand points required. The accuracy goal was 0.5% maximum error in $\beta^{\pm}$, which makes most values good to 0.1–0.2%.

In Fig. 4 we show the signal amplitude at resonance as a function of α for the three lowest-order truncation cases and the second-order power series. The latter is qualitatively wrong for α or $\alpha'>0.2$. The rate-equation approximation is qualitatively correct, but quantitatively high for $\alpha\gtrsim\frac{1}{2}$.

Case A is quite good for α up to 1 or 1.5 and fairly good at higher intensities. Case 1 is good for α up to 3 or 4. Similar results are found for the linewidths shown in Fig. 5. The rate-equation approximation always gives a narrower line, as can be seen even in the perturbation results (109)–(111) by neglecting γ_1. Case A is quite good. As in Fig. 1 the increase in width for $\alpha < \alpha'$ comes because we are then plotting the width of the shallower dip in the attenuation of the stronger beam.

For a fixed ratio α'/α, the square of the linewidth can often be well fitted by a linear function of power, even though the deviations are systematic. However, the extrapolation of such a fit to zero power comes out greater than γ_2. Therefore, using such a fit to remove power broadening from experimental data is subject to error, usually only a few percent, but as much as 25% error was found by fitting data for $\alpha = \alpha'$ up to $\alpha = 6$. To match the perturbation results (109)–(111), one might guess that the half-width $\tan\psi_{1/2} = (1 + 2\kappa\alpha + 2\kappa'\alpha')^{1/2}$. Although excellent at low powers, this formual trends high at high powers (7% at $\alpha = \alpha' = 1$, 13% at $\alpha = \alpha' = 4$). The three-parameter fit $\tan\psi_{1/2} = (1.05 + 1.50\alpha + 2.46\alpha')^{1/2}$, although a bit high at low-power levels, deviates from numerically calculated widths by not more than 2% for $\alpha' \leq \alpha \leq 1$ or for α up to 4 if $\alpha' < 0.5$. For larger $\alpha' < \alpha$, this formula is high; for $\alpha' > \alpha$, it is low unless both α and α' are small. To double the linewidth by power broadening requires α values ranging from 0.75 for $\alpha' = \alpha$ to 2.0 for small α'.

The line shape, although not exactly Lorentzian, can be well fitted by a Lorentzian curve.[88] Deviations are less than 1% of the depth for $\alpha \leq 1$, increasing to 2.5% at $\alpha = 4$. The line-splitting effect for β^+ in the rate-equation approximation appears to be masked by the inclusion of the reflection coefficient as no structure showed up in case B with α as large as 16.

In Fig. 6 we show the signal amplitude at resonance as a function of the strength α' of the probe beam. The slope of the curves at $\alpha' = 0$ is given by (121) but decreases appreciably by the time $\alpha' = 0.1$. The presence of a maximum in the curves followed by a slow decline shows that probe beam strengths should be no larger than necessary to achieve appreciable saturation.

In the above numerical calculations we have assumed equal relaxation rates $\gamma_a = \gamma_b = \gamma_1 = 1$ to bring out the effects of p_2. As the relaxation rates become unequal, γ_1 decreases and the results approach those of the rate-equation approximation, roughly in proportion to γ_1. In Figs. 4 and 5 the rate-equation approximation gives somewhat larger signal amplitudes and narrower lines, suggesting that unequal relaxations would be desirable experimentally. However, the comparison was made for fixed α, while from (17), (24), and (25) α varies with relaxation rates. Unequal relaxation rates may also permit the line-splitting effect of the rate-equation approximation to show up at sufficiently high powers.

H. Inclusion of Doppler Width

When the Doppler profile factor $e^{-\eta^2 y^2}$ is retained in the integrands, all calculations must be done numerically. The varying weight function distorts the wiggles shown in Fig. 3 so that area compensation is not as good. Therefore higher truncation cases are often required to maintain accuracy. The tails of the integrand are cut off by the Gaussian. As a function of a reciprocal variable, however, the tails have a more complex behavior and require more points for numerical integration.

Figure 7 shows the complete line shapes $\mathrm{Re}\beta^{\pm}$ for $\alpha = 1$, $\alpha' = 0.25$, and $\eta = 0.05$. Note that $\mathrm{Re}\beta^- \geq \mathrm{Re}\beta^+$, exactly the opposite of the stationary atom case. As η increases (assuming the other variables fixed[89]), β decreases. The signal amplitude and power broadening also decrease, but not appreciably until $\eta \gtrsim 0.3$. The dip in β^+ disappears for large η, although it may persist in β^- by evolving into the reflection-created dip for stationary atoms mentioned in Sec. IV A.

V. INTEGRATION OVER CELL LENGTH

Experimentally one does not measure the attenuation coefficient directly, but the change in amplitude of beams passing through finite lengths of absorbing medium. To determine the change theoretically one must integrate the propagation equations (45) or the corresponding equations for the dimensionless intensities

$$\frac{\partial \alpha}{\partial z} = -2\mathrm{Re}\beta^+ \alpha, \quad -\frac{\partial \alpha'}{\partial z} = -2\mathrm{Re}\beta^- \alpha'. \tag{140}$$

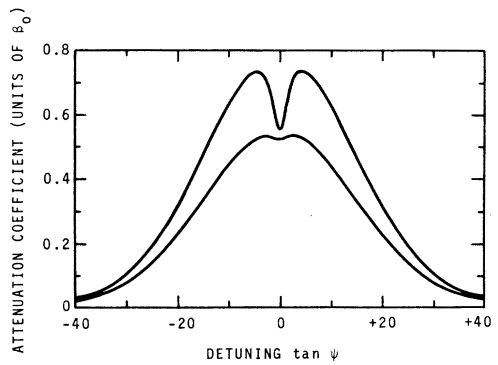

FIG. 7. Line shapes of attenuation coefficients for beam intensities $\alpha = 1$, $\alpha' = 0.25$ and Doppler parameter $\eta = 0.05$. The upper curve is $\mathrm{Re}\beta^-$ and the lower curve is $\mathrm{Re}\beta^+$.

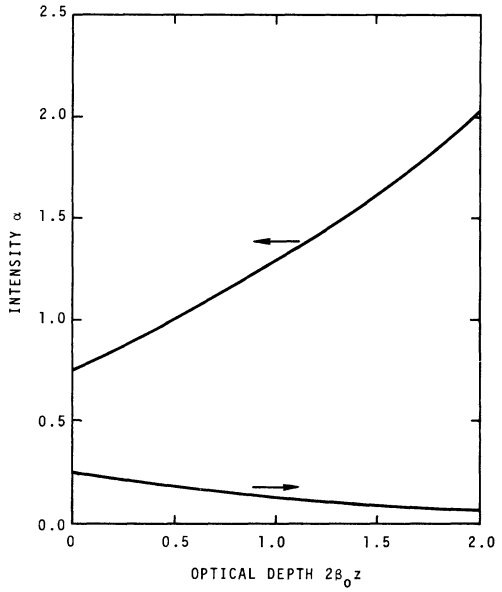

FIG. 8. Attenuation of two running waves traversing a long absorption cell. The arrows indicate the direction of propagation of the beams. The Doppler parameter η is 0.05 and the detuning $\tan\psi$ is 2.

For optically thin absorption cells we can consider $\beta^{\pm}$ constant and obtain

$$[\alpha(z)/\alpha(0)]-1=e^{-2\,\mathrm{Re}\,\beta^{+}z}-1\simeq-2\mathrm{Re}\beta^{+}z \qquad (141)$$

and a similar equation for α'. Therefore, optically thin cell measurements do approximately give the attenuation coefficients. For optically thick cells the changing intensities will change the attenuation coefficients and require that (140) be integrated as coupled nonlinear differential equations.

For a single running wave in an amplifying medium, the integration has been carried out by Rigrod[90] and in greater numerical detail by Bridges[91] for the limits of both homogeneous and inhomogeneous broadening. The first to consider the integration with two running waves were Ostrovskii and Yakubovich,[92] who used expressions equivalent to (50) and (51) for homogeneous broadening and obtained an implicit analytic result. Rigrod also considered two running waves,[93] but used

$$\beta^{+}=\beta^{-}=\beta_0/(1+2\alpha+2\alpha'),$$

corresponding to homogeneous broadening at resonance with no average over a wavelength. Karlov and Konev[94] integrated the Doppler-limit case far off resonance for which the waves are independent [see (136)] and Eqs. (140) are uncoupled. We have numerically integrated (140) in the general case where the coefficients have Lamb-dip features and must themselves be determined numerically as described in Sec. IV. The variation of the attenuation coefficients with α and α' is sufficiently slow that numerical integration works well, even with step sizes as large as $2\beta_0\Delta z=0.4$.

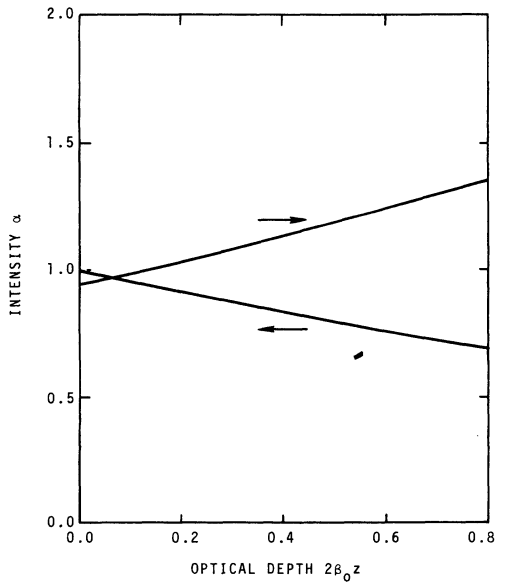

FIG. 9. Intensity variation of two running waves in a high-gain laser. The arrows indicate the direction of propagation of the beams, which are partially reflected at the boundaries of the figure. The Doppler parameter η is 0.05 and the system is tuned to resonance.

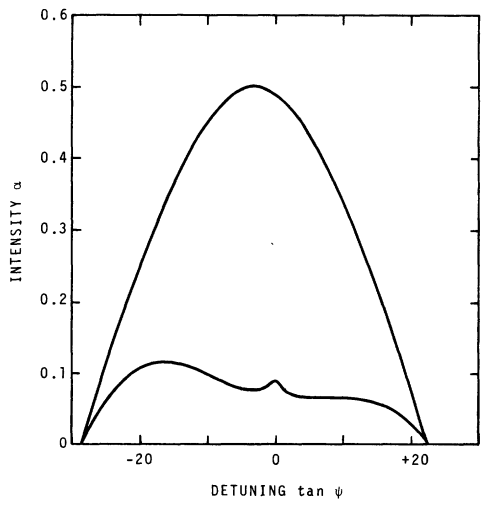

FIG. 10. Saturated absorption line shape for laser radiation traversing a medium and being reflected back on itself. The upper curve is an assumed input laser line shape and the lower curve is the output line shape after attenuation. The peak input intensity α is 0.5 occuring at a detuning $\tan\psi=3.08$ relative to the absorber resonance. The ratio of laser to absorber Doppler widths is 1.54, the Doppler parameter η is 0.05, and the optical depth $2\beta_0 z$ is 1.2.

In Fig. 8 we show a representative example of the attenuation of a saturating beam incident from the right and a weaker probe beam incident from the left as they pass through an optically thick absorption cell. The net absorption is 63% for the saturating beam and 76% for the probe beam, both detuned somewhat from resonance. The difference in absorption of the two beams is less at resonance (cf. Fig. 7). For a very weak nonsaturating beam, the absorption would be 86%. In Fig. 9 we show the intensity variation of two running waves that might occur within a high-gain laser oscillator having a 95% mirror on the left and a 50% mirror on the right. Such a system is not well described by the standing-wave small-gain theory.

Two methods have been used experimentally to obtain two oppositely running waves in an absorption cell external to the laser cavity. In the first method,[15,17,18,20,95] the laser beam is sent through the cell and relfected from a mirror back along the same path. In the second method,[16,23,77] the laser beam is split into a strong (saturating) beam and a weak (probe) beam, which are then directed into opposite ends of the cell. Both methods correspond mathematically to mixed-boundary conditions for (140). To solve them numerically it is necessary to guess the intensity of one (or both) beams at one end. One then integrates both intensities simultaneously to the other end and iterates until satisfactory agreement with the boundary conditions has been obtained. A semiempirical formula for guessing the amplitude of the stronger beam after traversing the cell has been developed and permits solving the mixed-boundary-value problem numerically with only two or three iterations for optical depths $2\beta_0 z$ up to about 4.6 (20 dB unsaturated attenuation).

In Fig. 10 we show a numerically generated line shape corresponding to the first method of observation. The upper curve is the input line shape of the laser source (here assumed to be a Gaussian truncated at half-height) and the lower curve is the output line shape after two passes through the cell. The broad depression is the Doppler line of the absorber,[96] while the small pip is the saturated absorption signal or "inverted Lamb dip." As the optical depth increases, the output becomes weaker, but the pip becomes a larger fraction of the background.

In Fig. 11 we show part of a numerically generated line shape corresponding to the second method of observation. The intensities correspond to those shown as a function of optical depth in Fig. 8. The upper curve shows the line shape of the weaker probe beam after traversing the absorption cell in the presence of the saturating beam. The dotted curve just beneath is the same line shape in the absence of the saturating beam. The lower curve is the difference between the two upper curves and can be the directly observed signal. Its height is 48% of the background, its width is broadened 30% by power, and it has 5% asymmetry. The asymmetry is due to the assumed form of the input laser line.

In Fig. 12 we show the probe beam intensity at resonance as a function of optical depth. The input intensities are held fixed. When the saturating beam is present (upper curve) the probe beam is attenuated less than when it is absent (lower curve). The difference signal first increases to a broad maximum about $2\beta_0 z \simeq 1$ (larger at higher input powers) and then decreases as the beam weakens in both cases. However, the ratio of the difference signal to its background (lower curve) increases monotonically.

The width of the signal line shape decreases with optical depth, partly because the sides of the line, being less saturated, are attenuated more than the peak of the line, but mostly because of reduced power broadening as the saturating beam is attenuated. Figure 13 shows the power broadening of the signal in the second method of observation for various optical depths, but with input power assumed independent of detuning. For optic-

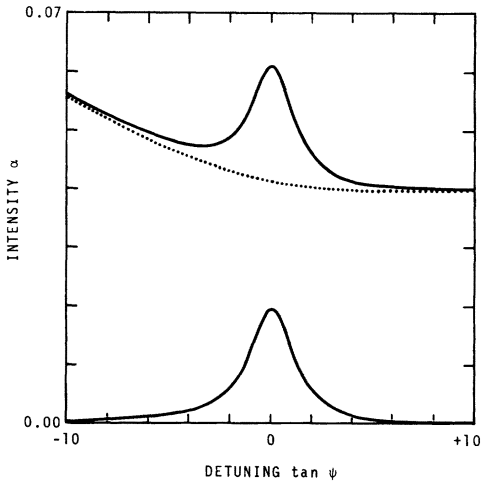

FIG. 11. Saturated absorption line shape for two overlapping beams directed into opposite ends of an absorption cell. The upper curve is the probe beam intensity after traversing the cell in the presence of the saturating beam, the dotted curve is the probe beam intensity in the absence of the saturating beam, and the lower curve is the difference between the two upper curves. The maximum input intensities α are 0.75 and 0.25 for the saturating and probe beams, respectively, at a detuning $\tan\psi = 2$ relative to the absorber resonance. The laser input line shapes (not shown) and Doppler widths are the same as in Fig. 10. The optical depth $2\beta_0 z$ is 2.

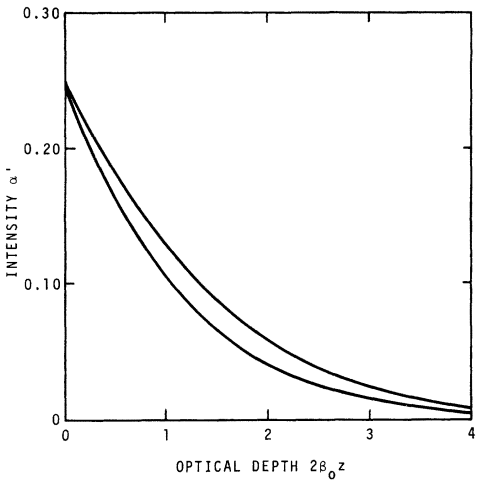

FIG. 12. Probe beam intensity as a function of optical depth. The upper curve shows the attenuation in the presence of the saturating beam, and the lower curve in its absence. The difference between the curves gives the saturated absorption signal amplitude. Input intensities are fixed at $\alpha = 0.72$ and $\alpha' = 0.25$ for the saturating and probe beams. Input frequencies are on resonance and the Doppler limit ($\eta = 0$) used.

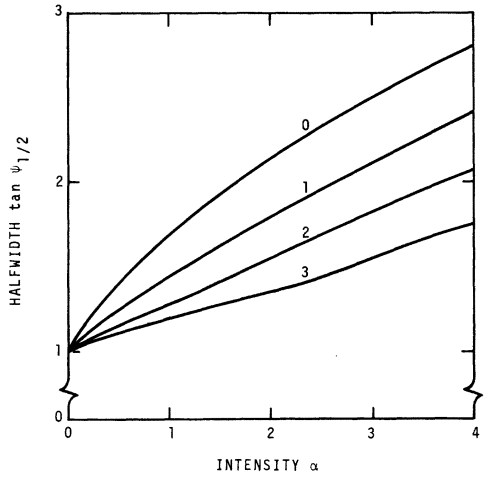

FIG. 13. Power broadening of saturated absorption signal in the Doppler limit for various optical depths $2\beta_0 z$ (indicated on the curves). The incident probe beam intensity is fixed at one-tenth the incident saturating beam intensity.

ally thin cells the square of the linewidth is a nearly linear function of power. For optical depths about $2\beta_0 z = 2$ the linewidth itself is more nearly linear. For large optical depths the slope of the linewidth versus power curve is decreasing at small and very large α, but may increase for intermediate values such that saturation effectively makes the medium no longer optically thick. In any case, extrapolation of the linewidth to zero power is unreliable unless data at very low powers (very weak signals) are available.

VI. EXPERIMENTAL IMPLICATIONS

In the design of saturated absorption experiments, whether for spectroscopy, line-broadening, or frequency-stability studies, one would like to maximize the signal while minimizing the power broadening. These goals are somewhat incompatible since we have found both signal and power broadening increase with power. The best compromise will depend on signal-to-noise considerations, but is probably with the intensity parameter α of the order of unity (moderate saturation). Comparing Figs. 4(a) and 5(a), for example, we find that when α is increased from 0.25 to 1.0, the signal amplitude increases 130% while power broadening increases only 30%. However, when α is increased from 1.0 to 4.0, the signal increases only an additional 45% with a corresponding 63% increase in linewidth. But the dependence on power is slow enough that power levels are not crucial.

The relative size of the saturation signal compared to the background intensity detuned from the saturation dip is increased both by observing the signal on a weak probe beam and by using a long absorption cell. Since power broadening is also thereby reduced, these are desirable experimental features, but should not be overdone. The absolute signal intensity must be large enough to be readily detected. The use of long cells may also present alignment and mode-matching difficulties such that geometric effects not considered in our analysis are important. For example, the signal strength will vary with the overlap of two beams of finite size, a problem studied by Kompanets and Letokhov in a simplified model.[97]

In studies involving pressure or lifetime broadening, power broadening must be carefully removed, preferably with data at low saturation levels. Deviations of observed power broadening from that predicted by our theory may be due either to effects of transverse geometry or the inapplicability of our relaxation model, for example, if pressures are low enough that atoms traverse a finite beam without collision.

ACKNOWLEDGMENT

The author wishes to thank Dr. F. R. Petersen for discussions and demonstrations of saturated absorption experiments.

[1]C. H. Townes, Phys. Rev. 70, 665 (1946).
[2]R. Karplus and J. Schwinger, Phys. Rev. 73, 1020 (1948).
[3]H. S. Snyder and P. I. Richards, Phys. Rev. 73, 1178 (1948).
[4]I. I. Rabi, Phys. Rev. 51, 652 (1937).
[5]A. Abragam, *The Principles of Nuclear Magnetism* (Clarendon, Oxford, England, 1961).
[6]A. Kastler, Phys. Today 20, No. 9, 34 (1967).
[7]For a good physical discussion of saturation in homogeneously broadened systems see A. Javan, Phys. Rev. 107, 1579 (1957).
[8]W. R. Bennett, Appl. Optics Suppl. 1, 24 (1962).
[9]S. G. Rautian and T. A. Germogenova, Opt. Spektrosk. 17, 157 (1964) [Opt. Spectrosc. 17, 85 (1964)].
[10]W. E. Lamb, Jr., Phys. Rev. 134, A1429 (1964).
[11]P. H. Lee and M. L. Skolnick, Appl. Phys. Lett. 10, 303 (1967).
[12]V. N. Lisitsyn and V. P. Chebotaev, Zh. Eksper. i Teor. Fiz. 54, 419 (1968) [Sov. Phys. JETP 27, 227 (1968)].
[13]C. Freed and A. Javan, Appl. Phys. Lett. 17, 53 (1970).
[14]T. Hänsch and P. Toschek, IEEE J. Quantum Electron. 4, 467 (1968).
[15]P. Rabinowitz, R. Keller, and J. T. LaTourette, Appl. Phys. Lett. 14, 376 (1969).
[16]C. Bordé, Compt. Rend. 271, 371 (1970).
[17]R. G. Brewer, M. J. Kelly, and A. Javan, Phys. Rev. Lett. 23, 559 (1969).
[18]M. W. Goldberg and R. Yusek, Appl. Phys. Lett. 17, 349 (1970).
[19]J. D. Knox and Y. H. Pao, Appl. Phys. Lett. 18, 360 (1971).
[20]E. E. Uzgiris, J. L. Hall, and R. L. Barger, Phys. Rev. Lett. 26, 289 (1971).
[21]M. D. Levenson and A. L. Schawlow, Phys. Rev. A 6, 10 (1972).
[22]T. Hänsch and P. Toschek, IEEE J. Quantum Electron. 5, 61 (1969).
[23]T. W. Hänsch, I. S. Shahin, and A. L. Schawlow, Phys. Rev. Lett. 27, 707 (1971).
[24]R. L. Barger and J. L. Hall, Phys. Rev. Lett. 22, 4 (1969).
[25]G. R. Hanes and K. M. Baird, Metrologia 5, 32 (1969).
[26]H. Hellwig, H. E. Bell, P. Kartaschoff, and J. C. Bergquist, J. Appl. Phys. 43, 450 (1972).
[27]S. Stenholm and W. E. Lamb, Jr., Phys. Rev. 181, 618 (1969).
[28]B. J. Feldman and M. S. Feld, Phys. Rev. A 1, 1375 (1970).
[29]H. K. Holt, Phys. Rev. A 2, 233 (1970).
[30]M. S. Feld and A. Javan, Phys. Rev. 177, 540 (1969).
[31]B. J. Feldman and M. S. Feld, Phys. Rev. A 5, 899 (1972).
[32]T. Hänsch and P. Toschek, Z. Physik 236, 213 (1970).
[33]J. H. Shirley, Am J. Phys. 36, 949 (1968).
[34]J. H. Shirley, Phys. Rev. 181, 600 (1969).
[35]Consideration of different polarizations also involves treatment of level degeneracy and can be considerably more complicated. See, for example, the theory of the Zeeman laser by M. Sargent, W. E. Lamb, Jr., and R. L. Fork [Phys. Rev. 164, 436 (1967)].
[36]H. Haken [in *Handbuch der Physik*, edited by S. Flügge (Springer, Berlin, 1970), Vol XXV] has previously used the δ functions to introduce spatial dependence, but did not consider velocity dependence.
[37]A. N. Oraevskii, Radiotekhnika i Elektronika 4, 718 (1959) [Radio Eng. Electron 4, 228 (1959)].
[38]E. T. Jaynes and F. W. Cummings, Proc. IEEE 51, 89 (1963).
[39]L. W. Davis, Proc. IEEE 51, 76 (1963).
[40]A. K. Popov, Zh. Eksper. i Teor. Fiz. 48, 1279 (1965) [Sov. Phys. JETP 21, 856 (1965)].
[41]N. L. Balazs and I. Tobias, Phil. Trans. Roy. Soc. London 264, 1 (1969).
[42]E. G. Pestov and S. G. Rautian, Zh. Eksper. i Teor. Fiz. 56, 902 (1969) [Sov. Phys. JETP 29, 488 (1969)].
[43]E. V. Baklanov and V. P. Chebotaev, Zh Eksper. i Teor. Fiz. 60, 552 (1971) [Sov. Phys. JETP 33, 300 (1971)].
[44]S. Haroche and F. Hartmann, Phys. Rev. A 6, 1280 (1972).
[45]J. H. Shirley, Phys. Rev. 138, B979 (1965).
[46]B. L. Gyorffy, M. Borenstein, and W. E. Lamb, Jr., Phys. Rev. 169, 340 (1968).
[47]T. Kan and G. J. Wolga, IEEE J. Quantum Electron. 7, 141 (1971).
[48]S. G. Rautian, Zh. Eksper. i Teor. Fiz. 51, 1176 (1966) [Sov. Phys. JETP 24, 788 (1967)].
[49]P. R. Berman and W. E. Lamb, Jr., Phys. Rev. A 2, 2435 (1970); 4, 319 (1971).
[50]A. Icsevgi and W. E. Lamb, Jr., Phys. Rev. 185, 517 (1969).
[51]B. D. Fried and S. D. Conte, *The Plasma Dispersion Function—Hilbert Transform of the Gaussian* (Academic, New York, 1961).
[52]E. I. Gordon, A. D. White, and J. D. Rigden, in *Proceedings of the Symposium on Optical Masers* (Polytechnic, Brooklyn, N. Y., 1963), p. 309.
[53]R. L. Carter and W. V. Smith, Phys. Rev. 73, 1053 (1948).
[54]The properties of a laser using Bragg reflection instead of mirrors for optical feedback have been studied [H. Kogelnik and C. V. Shank, J. Appl. Phys. 43, 2327 (1972)], but the possible origins of the assumed spatial inhomogeneity were not discussed.
[55]S. G. Rautian, in *Nonlinear Optics*, edited by D. V. Skobel'tsyn (Consultants Bureau, New York, 1970), p. 83; T. I. Kuznetsova, in *Nonlinear Optics* (Consultants Bureau, New York, 1970), p. 118.
[56]S. G. Rautian and I. I. Sobel'man, Zh. Eksper. i Teor. Fiz. 41, 456 (1961) [Sov. Phys. JETP 14, 328 (1962)].
[57]B. Senitzky and S. Cutler, Microwave J. 7, 62 (1964).
[58]N. Bloembergen and Y. R. Shen, Phys. Rev. 133, A37 (1964).
[59]T. I. Kuznetsova and S. G. Rautian, Zh. Eksper. i Teor. Fiz. 49, 1605 (1965) [Sov. Phys. JETP 22, 1098 (1966)].
[60]S. E. Schwarz and T. Y. Tan, Appl. Phys. Lett. 10, 4 (1967).
[61]E. V. Baklanov and V. P. Chebotaev, Zh. Eksper. i Teor. Fiz. 61, 922 (1971) [Sov. Phys. JETP 34, 490 (1972)].
[62]S. T. Scott, IEEE J. Quantum Electron. 4, 237 (1968).
[63]J. A. Fleck, J. Appl. Phys. 39, 3318 (1968).
[64]The use of the Fourier expansion in gas-laser theory is a concept apparently discovered independently by several authors (Refs. 27–29, 41, 62, 63), including the present one.
[65]H. S. Wall, *Analytic Theory of Continued Fractions*

(Van Nostrand, New York, 1948).
[66]H. Greenstein, Phys. Rev. 175, 438 (1968).
[67]F. Aronowitz, J. Appl. Phys. 41, 2453 (1970).
[68]F. Aronowitz, Phys. Rev. 139, A635 (1965).
[69]Yu. L. Klimontovich, P. S. Landa, and E. G. Larion-tsev, Zh. Eksper. i Teor. Fiz 52, 1616 (1967) [Sov. Phys. JETP 25, 1076 (1967)].
[70]C. Whitney, Phys. Rev. 181, 535 (1969).
[71]K. Takata, Japan J. Appl. Phys. 11, 699 (1972).
[72]A. P. Kazantsev, S. G. Rautian, and G. I. Surdutovich, Zh. Eksper. i Teor. Fiz. 54, 1409 (1968) [Sov. Phys. JETP 27, 756 (1968)].
[73]V. S. Letokhov, Zh. Eksper. i Teor. Fiz. 54, 1244 (1968) [Sov. Phys. JETP 27, 665 (1968)].
[74]V. S. Letokhov and B. D. Pavlik, Kvant. Elektron. 1, 53 (1971) [Sov. J. Quantum Electron. 1, 36 (1971)].
[75]H. Greenstein, J. Appl. Phys. 43, 1732 (1972).
[76]E. M. Garmire and A. Yariv, IEEE J. Quantum Electron. 3, 222 (1967).
[77]L. W. Davis, Phys. Rev. A 5, 2594 (1972).
[78]T. W. Hänsch, M. D. Levenson, and A. L. Schawlow, Phys. Rev. Lett. 26, 946 (1971).
[79]W. Culshaw, Phys. Rev. 164, 329 (1967).
[80]K. Uehara and K. Shimoda, Japan J. Appl. Phys. 4, 921 (1965).
[81]V. M. Tatarenkov, A. N. Titov, and A. V. Uspenskii, Opt. Spektrosk. 28, 572 (1970) [Opt. Spectrosc. 28, 306 (1970)].
[82]K. Shimoda and K. Uehara, Japan J. Appl. Phys. 10, 460 (1971).
[83]N. G. Basov, O. N. Kompanets, V. S. Letokhov, and V. V. Nikitin, Zh. Eksper. i. Teor. Fiz. 59, 394 (1970) [Sov. Phys. JETP 32, 214 (1971)].
[84]Recall, however, that we have assumed $\alpha\lambda$ small in the derivation of (120), and that the Doppler limit requires the saturation broadening to remain small compared to the Doppler width.
[85]S. Autler and C. H. Townes, Phys. Rev. 100, 703 (1955).
[86]*CRC Standard Mathematical Tables*, 14th ed., edited by S. M. Selby and B. Girling (The Chemical Rubber Co., Cleveland, 1964), p. 393.
[87]Note that this corresponds to setting $R_3 = 0$ and $T_2 = (1-\lambda)(F_1^- - \lambda F_1^+)$, i.e., retaining part of T_2.
[88]The author is indebted to Dr. J. L. Hall for applying his line-shape fitting program to some numerically generated data.
[89]Physically η cannot be changed without also changing β_0 or α, so it is important to specify which parameters are varied and which are held fixed.
[90]W. W. Rigrod, J. Appl. Phys. 34, 2602 (1963).
[91]W. B. Bridges, IEEE J. Quantum Electron. 4, 820 (1968).
[92]L. A. Ostrovskii and E. I. Yakubovich, Zh. Eksper. i Teor. Fiz. 46, 963 (1964) [Sov. Phys. JETP 19, 656 (1964)].
[93]W. W. Rigrod, J. Appl. Phys. 36, 2487 (1965).
[94]N. V. Karlov and Yu. B. Konev, Radio Eng. and Elect. Phys. 13, 491 (1968).
[95]F. Shimizu, Appl. Phys. Lett. 14, 378 (1969).
[96]The Doppler width of the laser is taken to be 1.54 times that of the absorber, corresponding to CO_2 laser radiation absorbed by SiF_4 [F. R. Petersen and B. L. Danielson, Bull. Am. Phys. Soc. 15, 1324 (1970)].
[97]O. N. Kompanets and V. S. Letokhov, Zh. Eksp. Teor. Fiz. Pis'ma Red. 14, 20 (1971)[JETP Lett. 14, 12 (1971)].

PHYSICAL REVIEW A VOLUME 8, NUMBER 1 JULY 1973

Liquid-Aluminum Structure Factor by Neutron Diffraction*

J. M. Stallard
Naval Ordnance Laboratory, Silver Spring, Maryland 20910

C. M. Davis, Jr.†
American University, Washington, D.C. 20016

(Received 4 January 1973)

The structure factor $S(Q)$ for liquid aluminum was measured at 703 and 1029 °C in the region $0 < Q < 15$ Å^{-1} using neutron-diffraction techniques. A description of the experimental apparatus and procedure is presented, as well as the method of reducing the neutron intensity to the structure factor. The results are compared with other simple liquid metals, and the electrical resistivity is calculated using the Ziman formulation. Excellent agreement is obtained between calculated and experimentally observed resistivity, both in absolute value and in temperature dependence. This agreement lends credence to both the measured structure factor and to the Ziman formulation for resistivity.

I. INTRODUCTION

Over the past decade highly successful statistical-mechanical approaches have been developed for predicting the properties of liquified inert gases.[1] Recently these techniques have been combined with various model potentials and used to calculate the thermodynamic and electrical properties of liquid metals.[2,3] In these calculations, the concept of a radial distribution function $g(r)$, or its transform, the structure factor $S(Q)$, and their temperature dependences are used. Neutron diffraction offers the most direct experimental means for obtaining the above quantities.